



NAS CR-120865
WANL-M-FR-72-012
DECEMBER 1972

(NASA-CR-120865) METALLURGICAL EVALUATION
OF FACTORS INFLUENCING THE DUCTILITY OF
AGED T-111 Final Report (Westinghouse
Astronuclear Lab., Pittsburgh) 89 p HC
\$6.50

N73-18540

Unclass
64240

CSC 11F G3/17

FINAL REPORT

METALLURGICAL EVALUATION OF FACTORS INFLUENCING THE DUCTILITY OF AGED T-111

BY

R. E. GOLD



WESTINGHOUSE ASTRONUCLEAR LABORATORY

CONTRACT NAS 3-15560

prepared for

NATIONAL AERONAUTICS AND SPACE ADMINISTRATION

NASA LEWIS RESEARCH CENTER

CLEVELAND, OHIO 44135

45

NOTICE

This report was prepared as an account of Government-sponsored work. Neither the United States, nor the National Aeronautics and Space Administration (NASA), nor any person acting on behalf of NASA:

- A.) Makes any warranty or representation, expressed or implied, with respect to the accuracy, completeness, or usefulness of the information contained in this report, or that the use of any information, apparatus, method, or process disclosed in this report may not infringe privately-owned rights; or
- B.) Assumes any liabilities with respect to the use of, or for damages resulting from the use of, any information, apparatus, method or process disclosed in this report.

As used above, "person acting on behalf of NASA" includes any employee or contractor of NASA, or employee of such contractor, to the extent that such employee or contractor of NASA or employee of such contractor prepares, disseminates, or provides access to any information pursuant to his employment or contract with NASA, or his employment with such contractor.

Request for copies of this report should be referred to

National Aeronautics and Space Administration
Scientific and Technical Information Facility
P. O. Box 33
College Park, Maryland 20740

1. Report No. NAS CR-120865		2. Government Accession No.		3. Recipient's Catalog No.	
4. Title and Subtitle Metallurgical Evaluation of Factors Influencing the Ductility of Aged T-111				5. Report Date December, 1972	
				6. Performing Organization Code	
7. Author(s) R. E. Gold				8. Performing Organization Report No. WANL-M-FR-72-012	
				10. Work Unit No.	
9. Performing Organization Name and Address Westinghouse Astronuclear Laboratory P. O. Box 10864 Pittsburgh, Pennsylvania 15236				11. Contract or Grant No. NAS 3-15560	
				13. Type of Report and Period Covered Contractor Report	
12. Sponsoring Agency Name and Address National Aeronautics and Space Administration Washington, D. C. 20546				14. Sponsoring Agency Code	
15. Supplementary Notes Project Manager, Paul E. Moorhead, Materials and Structures Division, NASA Lewis Research Center, Cleveland, Ohio					
16. Abstract <p>The metallurgical factors influencing the ductility of T-111 (Ta-8W-2Hf) alloy following long-time exposures of GTA welds and tubing in the temperature range 982°C (1800°F) through 1316°C (2400°F) were evaluated by means of scanning and transmission electron microscopy, Auger electron emission spectroscopy, and optical metallographic procedures.</p> <p>No classical aging response occurs in the alloy over the temperature range studied. The ductility impairment implied by previous investigations is not the result of microstructural response of the alloy to thermal exposures. Intergranular failure in the GTA sheet welds appears the result of random contamination by silicon, potassium, and/or fluorine at the grain boundaries of the fusion zones. Exposure to lithium at high temperatures had no adverse effects on the ductility of T-111 tubing. These materials were, however, sensitive to post-age handling and testing procedures.</p>					
17. Key Words (Suggested by Author(s)) T-111 (Ta-8W-2Hf) Ductility GTA Sheet Welds				18. Distribution Statement Unclassified - unlimited	
19. Security Classif. (of this report) Unclassified		20. Security Classif. (of this page) Unclassified		21. No. of Pages 79	
				22. Price* 6.50 2.00	

* For sale by the National Technical Information Service, Springfield, Virginia 22151

FOREWORD

This program was conducted by the Westinghouse Astronuclear Laboratory under NASA Contract NAS 3-15560. Mr. P. E. Moorhead of the NASA Lewis Research Center, Materials and Structures Division, was the NASA Project Manager for the program.

Special appreciation and recognition are extended to Dr. J. A. Cornie and Mr. C. W. Hughes of the Materials Department, Westinghouse Research and Development Center for their assistance with the transmission and scanning electron microscopy contained in this report. Similar appreciation is extended to Drs. P. W. Palmberg and R. E. Weber of Physical Electronics Industries, Edina, Minnesota without whose efforts the performance and interpretation of the Auger electron emission spectroscopy would not have been possible.

TABLE OF CONTENTS

	<u>Page No.</u>
1.0 SUMMARY	1
2.0 INTRODUCTION	3
3.0 TECHNICAL PROGRAM	5
3.1 Background	5
3.2 Specimen Identification	8
3.3 Procedures	11
4.0 RESULTS	20
4.1 Aged GTA Sheet Welds	20
4.2 Aged T-111 Tubing	51
5.0 DISCUSSION	68
5.1 Aged GTA Sheet Welds	68
5.2 Aged T-111 Tubing	71
6.0 CONCLUSIONS	74
7.0 RECOMMENDATIONS	77
8.0 REFERENCES	78

LIST OF ILLUSTRATIONS

<u>Figure No.</u>	<u>Title</u>	<u>Page No.</u>
1	Program Outline.	6
2	Geometry of GTA Weld Specimens Used for Bend Fracture Evaluations.	12
3	Geometry of T-111 Tube Specimens Used for Bend Fracture Evaluations.	13
4	Geometry of Specimens Used for Auger Spectroscopic Analysis.	14
5	Electron Energy Diagram Comparing Transitions Giving Rise to X-Ray and Auger Electron Emissions.	17
6	Microstructure of GTA Weld Specimen 1.	21
7	Scanning Electron Micrographs of Fracture Surface of GTA Weld Specimen 1; Fractured at $-196^{\circ}\text{C}(-320^{\circ}\text{F})$.	22
8	Microstructure of GTA Weld Specimen 2.	25
9	Scanning Electron Micrographs of Fracture Surface of GTA Weld Specimen 2; Fractured at $-196^{\circ}\text{C}(-320^{\circ}\text{F})$.	26
10	Transmission Electron Micrograph of Weld Zone Structure in GTA Weld Specimen 2.	27
11	Microstructure of GTA Weld Specimen 3.	28
12	Scanning Electron Micrographs of Fracture Surface of GTA Weld Specimen 3; Fractured at $-196^{\circ}\text{C}(-320^{\circ}\text{F})$.	29
13	Scanning Electron Micrographs of Fracture Surface of GTA Weld Specimen 3; Fractured in Auger Apparatus at $-150^{\circ}\text{C}(-238^{\circ}\text{F})$.	30
14	Microstructure of GTA Weld Specimen 4.	32
15	Scanning Electron Micrographs of Fracture Surface of GTA Weld Specimen 4; Fractured at $-196^{\circ}\text{C}(-320^{\circ}\text{F})$.	33
16	Microstructure of GTA Weld Specimen 5.	34
17	Scanning Electron Micrographs of Fracture Surface of GTA Weld Specimen 5; Fractured at $-196^{\circ}\text{C}(-320^{\circ}\text{F})$.	36
18	Transmission Electron Micrograph of GTA Weld Specimen 5.	37
19	Microstructure of GTA Weld Specimen 6.	38
20	Scanning Electron Micrographs of Fracture Surface of GTA Weld Specimen 6; Fractured at $-196^{\circ}\text{C}(-320^{\circ}\text{F})$.	39

LIST OF ILLUSTRATIONS (Continued)

<u>Figure No.</u>	<u>Title</u>	<u>Page No.</u>
21	Transmission Electron Micrograph of GTA Weld Specimen 6.	40
22	Microstructure of GTA Weld Specimen 7.	41
23	Scanning Electron Micrographs of Fracture Surface of GTA Weld Specimen 7; Fractured at $-196^{\circ}\text{C}(-320^{\circ}\text{F})$.	42
24	Microstructure of GTA Weld Specimen 8.	44
25	Scanning Electron Micrographs of Fracture Surface of GTA Weld Specimen 8; Fractured at $-196^{\circ}\text{C}(-320^{\circ}\text{F})$.	45
26	Microstructure of GTA Weld Specimen 9.	46
27	Scanning Electron Micrographs of Fracture Surface of GTA Weld Specimen 9; Fractured at $-196^{\circ}\text{C}(-320^{\circ}\text{F})$.	47
28	Transmission Electron Micrograph of GTA Weld Specimen 9.	48
29	Transmission Electron Micrographs of GTA Weld Specimen 9.	49
30	Microstructure of GTA Weld Specimen 10.	50
31	Scanning Electron Micrographs of Fracture Surface of GTA Weld Specimen 10; Fractured at $-196^{\circ}\text{C}(-320^{\circ}\text{F})$.	52
32	Scanning Electron Micrographs of Fracture Surface of GTA Weld Specimen 10; Fractured in Auger Apparatus at $-150^{\circ}\text{C}(-238^{\circ}\text{F})$.	53
33	Transmission Electron Micrograph of GTA Weld Specimen 10.	54
34	As-Aged Microstructure of T-111 Tube Specimen 11.	55
35	Scanning Electron Micrographs of Fracture Surface of T-111 Tube Specimen 11; Fractured at $-196^{\circ}\text{C}(-320^{\circ}\text{F})$.	56
36	Scanning Electron Micrographs of Fracture Surface of T-111 Tube Specimen 11; Fractured in Auger Apparatus at $-150^{\circ}\text{C}(-238^{\circ}\text{F})$. Annealed 1 Hour- $982^{\circ}\text{C}(1800^{\circ}\text{F})$ Prior to Testing.	58
37	Scanning Electron Micrographs of Fracture Surface of T-111 Tube Specimen 11; Fractured in Auger Apparatus at $-150^{\circ}\text{C}(-238^{\circ}\text{F})$. Not Annealed Prior to Testing.	59
38	Transmission Electron Micrograph of T-111 Tube Specimen 11.	60

LIST OF ILLUSTRATIONS (Continued)

<u>Figure No.</u>	<u>Title</u>	<u>Page No.</u>
39	As-Aged Microstructure of T-111 Tube Specimen 12.	63
40	Scanning Electron Micrographs of Fracture Surface of T-111 Tube Specimen 12; Fractured at $-196^{\circ}\text{C}(-320^{\circ}\text{F})$.	64
41	Scanning Electron Micrographs of Fracture Surface of T-111 Tube Specimen 12; Fractured in Auger Apparatus at $-150^{\circ}\text{C}(-238^{\circ}\text{F})$. Annealed 1 Hour- $982^{\circ}\text{C}(1800^{\circ}\text{F})$ Prior to Testing.	65
42	Scanning Electron Micrographs of Fracture Surface of T-111 Tube Specimen 12; Fractured in Auger Apparatus at $-150^{\circ}\text{C}(-238^{\circ}\text{F})$. Not Annealed Prior to Testing.	66

LIST OF TABLES

<u>Table No.</u>	<u>Title</u>	<u>Page No.</u>
1	Program Specimen Identification.	9
2	Program Specimen Chemistry Data.	10
3	Results of Auger Analyses on GTA Weld Specimens.	23
4	Results of Auger Analyses on T-111 Tubing Specimens.	62
5	Summary of GTA Weld Specimen Fracture Behavior.	69
6	Summary of T-111 Tube Specimen Fracture Behavior.	72

1.0 SUMMARY

A metallurgical evaluation of the factors influencing the ductility of T-111 (Ta-8W-2Hf) alloy after long-time elevated temperature exposures was performed. Gas tungsten-arc (GTA) sheet welds aged in ultra-high vacuum and tubing material exposed to lithium on the inside diameter and vacuum environments on the outside were evaluated. Exposure conditions included times to 10,000 hours in the temperature range 982°C (1800°F) through 1316°C (2400°F). The effect of 1 hr. -1982°C (3600°F) post-age annealing was also considered. Following low temperature fracture, specimens were characterized and examined by means of scanning and transmission electron microscopy, Auger electron emission spectroscopy and optical metallographic procedures.

Previous investigations of the bend ductility of aged GTA welds and alkali metal-exposed T-111 tubing had suggested the possibility of significant ductility impairment following long-time exposures in the temperature range 982°C (1800°F) through 1149°C (2100°F). Premature intergranular failures were noted to occur as high as -18°C (0°F) whereas unexposed T-111 typically displays full bend behavior to -196°C (-320°F). Certain results of the prior studies had suggested the possibility a classical aging reaction might be occurring in the weld fusion zones.

Scanning electron microscopy studies proved invaluable for the characterization of the fracture surfaces, permitting definitive interpretation of the various fracture morphologies. Transmission electron microscopy was used to characterize dislocation structure and to determine the extent and possible role of precipitation on the behavior of the aged alloy. Freshly fractured surfaces were examined for the presence of segregation at the fracture surface by means of Auger electron emission spectroscopy.

The experimental evaluations reveal no "problem" temperature range exists which must be avoided for long-time exposures. No evidence was obtained to support the original hypothesis that a solid-state aging reaction was occurring in the weld fusion zones. Of the aged

GTA welds evaluated, representing ten different thermal histories, only three specimens exhibited what may be described as a tendency toward intergranular failure. In each of these three specimens contamination by silicon, potassium and/or fluorine was detected at the fusion zone grain boundaries.

The aged tube materials were found to have suffered no loss of ductility due to the high temperature lithium exposures. Earlier observations of intergranular fracture in the specimen exposed at 1038°C (1900°F) can be attributed to an enhanced sensitivity to post-age handling and/or testing. These results are consistent with the results of other workers regarding the sensitivity of aged T-111 to post-age handling. The results of this program indicate that T-111 can be exposed for long periods at temperatures up to at least 1316°C (2400°F) without loss of ductility provided care is exercised in subsequent post-age handling operations.

2.0 INTRODUCTION

This report presents the results of a metallurgical evaluation of the factors affecting the ductility of the tantalum-base alloy T-111 (Ta-8W-2Hf) following long-time exposures at temperatures ranging from 982°C (1800°F) through 1316°C (2400°F).

Results of bend tests on aged T-111 have indicated a propensity toward grain boundary failure at temperatures as high as -18°C (0°F)⁽¹⁾. This contrasts with the normal full 100° bends obtained at -196°C (-320°F) with unaged T-111. While primarily associated with GTA sheet welds, similar behavior has also been observed in room temperature ring flattening tests on T-111 tubing following exposure in liquid alkali metal systems operated for long times at 1038°C (1900°F). The behavior observed is somewhat different than classical ductile-brittle transition behavior in body-centered-cubic metals in that the fracture mode changes from transgranular shear to one which is mainly intergranular rather than to transgranular cleavage.

Several aspects of the aging response suggested the possibility a classical aging reaction might be occurring in the weld fusion zone. In particular, the fact no response was observed for specimens aged above 1149°C (2100°F) or for specimens given a "homogenizing" post-weld anneal above 1760°C (3200°F) implied the aging response might be associated with the inhomogeneous weld fusion zone microstructures. If such were the case, detailed microstructural investigations of the subject specimens should reveal the responsible factors.

Specimens were selected to include those aging conditions producing the most severe ductility loss as well as conditions which were found to have no adverse effect on bend ductility. With the exception of two specimens of T-111 tubing exposed at 1038°C (1900°F) and 1227°C (2240°F) for periods to 10,000 hours, all specimens were GTA sheet welds.

Analytical techniques used in the evaluation of specimens for this program included scanning electron microscopy, transmission electron microscopy and Auger electron emission

spectroscopy in addition to normal optical metallographic procedures. Specimens were prepared for evaluation by means of bend fracturing at $-196^{\circ}\text{C}(-320^{\circ}\text{F})$ except in the case of the Auger specimens which were fractured at $-150^{\circ}\text{C}(-238^{\circ}\text{F})$, the lowest temperature attainable with currently available equipment.

3.0 TECHNICAL PROGRAM

The outline of the technical evaluation program pursued is provided in Figure 1.

3.1 Background

Gas tungsten-arc (GTA) welds in T-111 are quite ductile with full 100° 1t bends being routinely achieved at $-196^{\circ}\text{C}(-320^{\circ}\text{F})$ in the as welded or as welded plus 1 hour- 1316°C (2400°F) post-weld annealed condition. However, previous studies on Contract NAS 3-2540⁽¹⁾ of the elevated temperature stability of refractory metal alloys have indicated GTA weld structures in T-111 sheet are subject to a discernible change in low temperature bend test performance following long-time exposures at 982° to 1149°C (1800° to 2100°F) in ultra-high vacuum. The temperature for weld tearing in the 1t bend test of aged GTA welds was found to increase to as high as $-18^{\circ}\text{C}(0^{\circ}\text{F})$. More recent studies, on Contract NAS 3-11827⁽²⁾, using 1000 hour- 1149°C (2100°F) aging in ultra-high vacuum, indicated a much less severe loss of low temperature bend ductility. In the latter program 1t bend transition temperatures of the aged welds ranged from -101° to -157°C (-150° to -250°F). One of the objectives of the present program was to provide an explanation for the difference in the results of the two programs. Other results of these investigations include:

- No base metal response was noted for any of the thermal exposures employed. In itself, this does not preclude the possibility of aging in base metal. However, if such aging is occurring the resulting 1t bend DBTT is still below $-196^{\circ}\text{C}(-320^{\circ}\text{F})$, the lowest test temperature used.
- No loss of ductility was observed in tensile tests conducted at room temperature and above.
- Notched tensile tests performed on aged GTA weld specimens indicated no notch sensitivity* to temperatures as low as $-196^{\circ}\text{C}(-320^{\circ}\text{F})$.

* That is, the notch-strength-ratios were consistently > 1.0 .

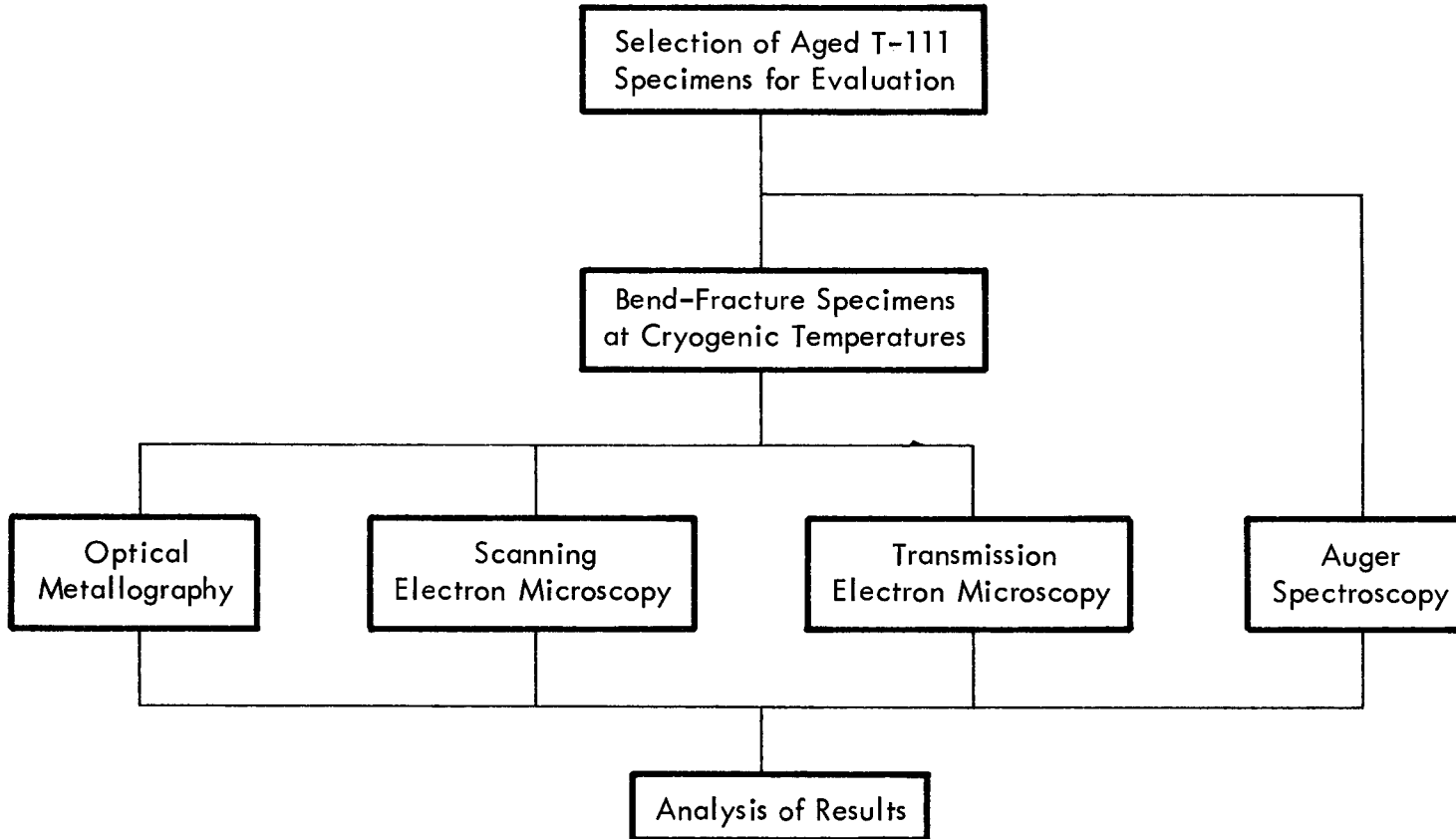


FIGURE 1. Program Outline

- Failure does not occur by catastrophic fracture, but rather by a slowly propagating grain boundary "tearing" process, invariably located in the oriented grain structure of the weld fusion zone.

A review of the preceding observations indicates the problem is probably not of extreme engineering significance since most common engineering tests do not corroborate the implied ductility loss. However, the possibility that further degradation could result in similar behavior at room temperature or above is, on the other hand, quite serious since the excellent formability of T-111 base and weld metal is one of the alloy's most attractive properties.

Observations have been made of an apparently similar loss of bend ductility in T-111 tubing exposed to lithium or potassium for long periods in the 982° to 1038°C (1800° to 1900°F) temperature range⁽³⁾. Post-exposure evaluation of T-111 tubing used in such systems includes a ring flattening test whereby 0.64 cm. (0.25 in.) sections of 2.54 cm. (1.0 in.) diameter tubing are crushed by radial pressure (commonly in a vise). Following certain exposure conditions these flattening tests result in catastrophic intergranular failure whereas unexposed T-111 tubing can be completely flattened without incident.

While the intergranular fracture mode observed in the ring flattening tests suggests a similar aging effect as that implied by the aged GTA weld results, certain differences are also evident. These include:

- The tests on the T-111 tubing are on fine-grained base metal rather than coarse-grained GTA welds.
- The fractures occur during flattening at room temperature, a temperature where the aged GTA welds display full bend ductility.
- The presence of liquid potassium or lithium introduces the possibility of contamination during aging.

In addition, certain peculiarities in the behavior of the tubing exposed to liquid alkali metals suggests a possible influence of the conditions and procedures used in preparing the specimens for testing. Conversely, the more controlled conditions under which the aged GTA weld data were accumulated would seem to favor an explanation based on the metallurgical response of the alloy to the thermal exposures.

3.2 Specimen Identification

Specimens representing a total of twelve different thermal exposure histories were chosen for evaluation. These specimens were supplied from three previous NASA-sponsored contracts. All but two specimens were from GTA welded 0.062 cm.(0.035 in.) T-111 sheet. The remaining two specimens represented T-111 tubing which had been used in alkali metal loops operated at 1038°C(1900°F) and 1227°C(2240°F).

Details of the thermal history of the various specimens are provided in Table 1 along with previously determined 1t bend DBTT's where available. The pre-age thermal treatments indicated in Table 1 are in addition to the 1 hour-1649°C(3000°F) recrystallization anneal used as the final processing step for this alloy. The original contracts from which individual specimens were supplied are also identified.

From Table 1 it can be seen that several specimens differ only in the use of a final post-age anneal in ultra-high vacuum at 1982°C(3600°F) for 1 hour. This heat treatment was used where duplicate specimens were available in order to assess its effect on the bend and fracture behavior. Specimens 1 through 10 were aged in an ultra-high vacuum environment. Specimens 11 and 12 differed somewhat in that they had been exposed to ultra-high vacuum on their OD surfaces and lithium on the ID surfaces.

The results of pre-age chemical analyses, and where available post-age analyses for C, O and N, are presented in Table 2. Although only spot-checks were performed after aging the results of Table 2 indicate no significant changes occurred on aging which could be responsible for the effects observed.

Table 1. Program Specimen Identification.

Specimen Number	Thermal History			Aged 1 $\frac{1}{2}$ DBTT °C (°F) (b)	Original Contract (b)
	1 hr. Pre-Age	Age Conditions	1 hr. Post-Age		
1	1316°C(2400°F)	1000 Hrs. -982°C(1800°F)	—	-157 (-250)	NAS 3-2540
2	"	"	1982°C(3600°F)	-157 (-250)	"
3	"	5000 Hrs. -1149°C(2100°F)	—	< -18 (< 0)	"
4	"	10000 Hrs. -1149°C(2100°F)	—	< -18 (< 0)	"
5	"	"	1982°C(3600°F)	< -18 (< 0)	"
6	"	10000 Hrs. -1316°C(2400°F)	—	< -196 (< -320)	"
7	"	"	1982°C(3600°F)	< -196 (< -320)	"
8	"	1000 Hrs. -1149°C(2100°F)	—	-143 (-225)	NAS 3-11827
9	"	"	1982°C(3600°F)	-143 (-225)	"
10	1982°C(3600°F)	"	—	-157 (-250)	"
11	1316°C(2400°F)	7500 Hrs. -1038°C(1900°F)	—	N. D.	NAS 3-6474
12	"	10000 Hrs. -1227°C(2240°F)	—	N. D.	"

N. D. = Not determined

(a) All post-age anneals in ultra-high vacuum ($< 10^{-8}$ torr).

(b) NAS 3-2540 ; Determination of Weldability and Elevated Temperature Stability of Refractory Metal Alloys (See reference 1)

NAS 3-11827; Influence of Restraint and Thermal Exposure on Welds in T-111 and ASTAR-811C (See reference 2)

NAS 3-6474; Advanced Refractory Alloy Corrosion Loop Program (See reference 3)

Table 2. Program Specimen Chemistry Data

Specimen Number	Original Contract	Heat Number	Aging Conditions	Pre-Age Chemistry ^(a)						Post-Age Chem. ^(a)		
				Ta	W	Hf	C	O	N	C	O	N
1	3-2540	6-65042	1000 hrs-982°C	Bal	8.8	2.0	48	15	18	N. D.		
2	"	"	"			"				"		
3	"	"	5000 hrs-1149°C			"				"		
4	"	"	10000 hrs-1149°C			"				53	13	23
5	"	"	"			"				"	"	"
6	"	"	10000 hrs-1316°C			"				45	20	21
7	"	"	"			"				"	"	"
8	3-11827	650043	1000 hrs-1149°C	Bal	8.3	2.0	33	40	12	N. D.		
9	"	"	"			"				"		
10	"	"	"			"				"		
11	3-6474	N. A.	7500 hrs-1038°C			N. A.				N. A.		
12	"	"	10000 hrs-1227°C			"				"		

N. A. = Not Available.

N. D. = Not Determined.

(a) Metal analyses in wt. percent ; interstitial analyses (C, O, N) in wt. ppm.

3.3 Procedures

Specimen Preparation

Specimen configurations were dictated by the availability of material from the previous experimental programs. Thus, material used for the aged welds evaluated on this program was taken from sheet containing either longitudinal (specimens 4,5,8 and 9) or transverse (specimens 1,2,3,6,7 and 10) GTA welds. Details of the specimen geometry for these two cases are shown in Figure 2. All specimen blanking required was accomplished by means of shearing at room temperature. No edge cracking or other visible defects resulted from this operation.

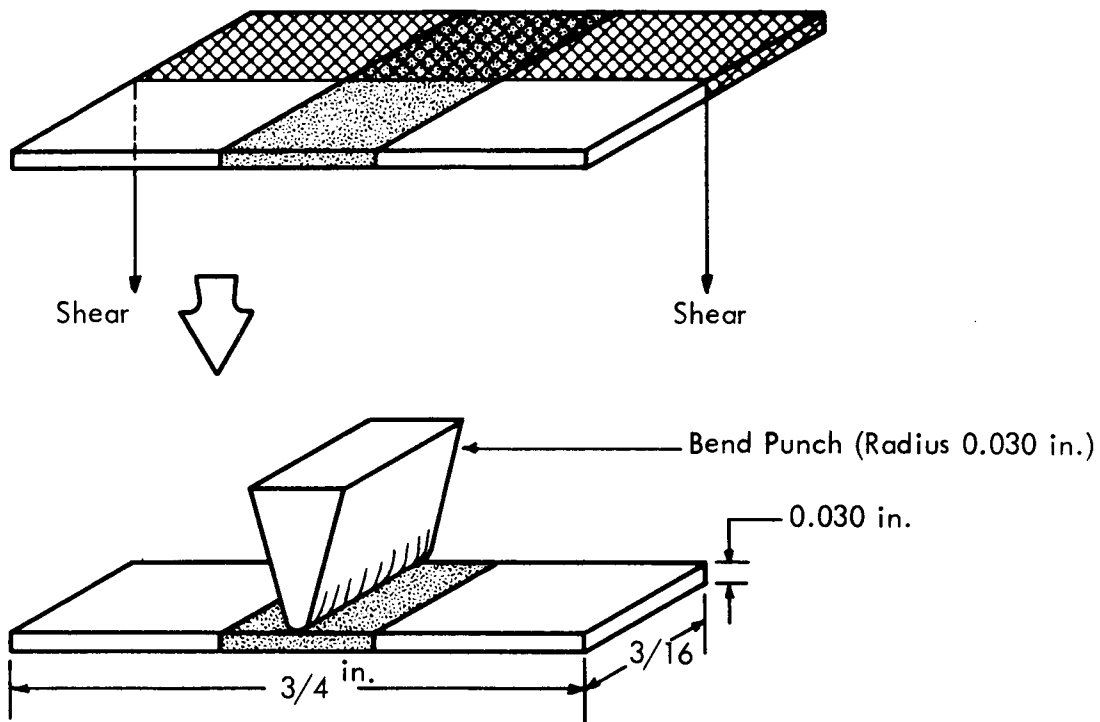
Material from the alkali metal corrosion loop program was supplied in the form of approximately 2.54 cm.(1.0 in.) long pieces of 2.54 cm.(1.0 in.) OD x 0.254 cm.(0.10 in.) wall thickness T-111 tubing. The specimen configuration used for the bend fracture evaluation of this material is shown in Figure 3. The notches indicated (Figure 3) were machined to facilitate fracture of the heavy walled tube specimens.

All of the preceding information pertains only to those specimens bend-fractured at $-196^{\circ}\text{C}(-320^{\circ}\text{F})$. These specimens were tested after the indicated shearing or machining, without heat treatment of any type. This point is made at this time because of some variance from this procedure for several of the Auger specimens. This will be elaborated upon later.

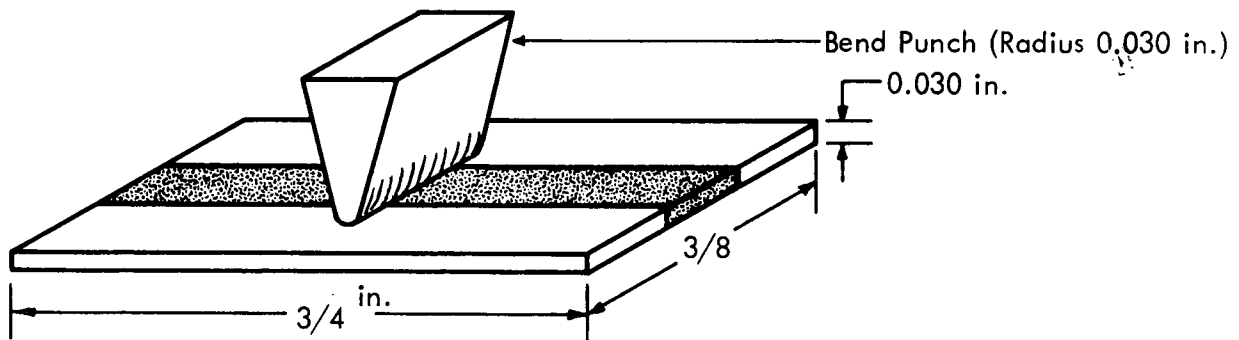
Specimens were prepared for Auger electron emission analysis using the specimen configurations shown in Figure 4. Specific reference to the configuration appropriate for a particular specimen will be made in the Results section of this report.

Bend Fracturing of Specimens

All bend fracturing was performed in liquid nitrogen at $-196^{\circ}\text{C}(-320^{\circ}\text{F})$. Despite the implied ductility loss in these specimens, several had to be bent in reverse in order to achieve complete fracture. GTA weld specimens were bent with the top surface of the weld



a) Transverse Weld Specimen



b) Longitudinal Weld Specimen

FIGURE 2. Geometry of GTA Weld Specimens Used for Bend Fracture Evaluations.

Piece shown is longitudinal slice removed from
tubing with water-cooled cutoff wheel.

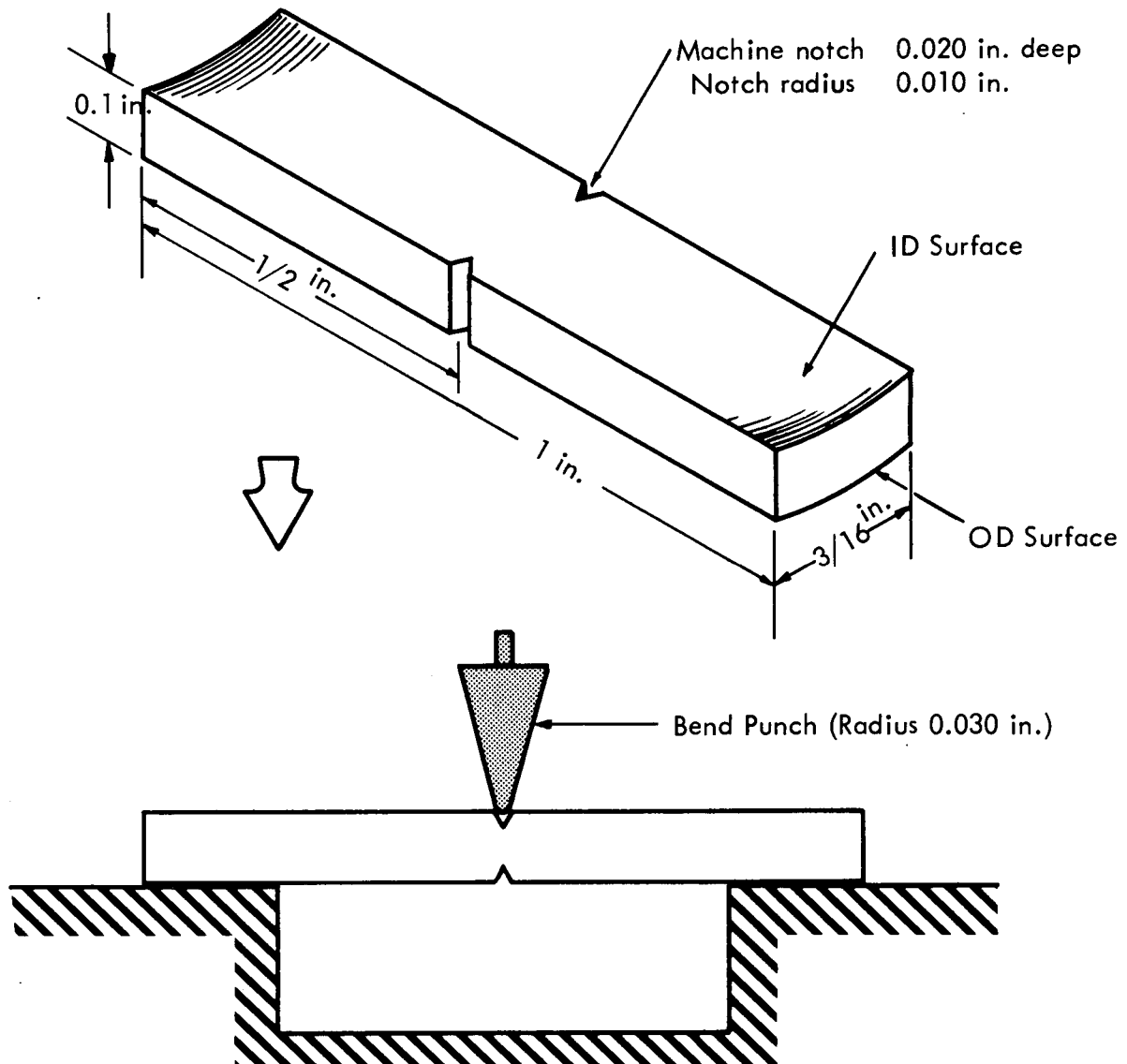


FIGURE 3. Geometry of T-111 Tube Specimens Used for
Bend Fracture Evaluations.

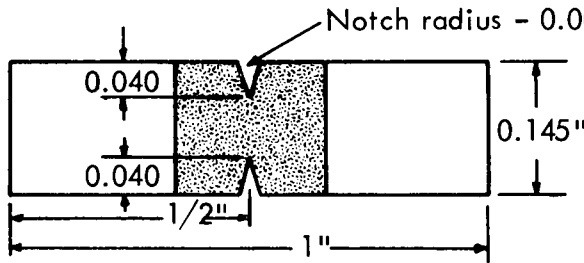
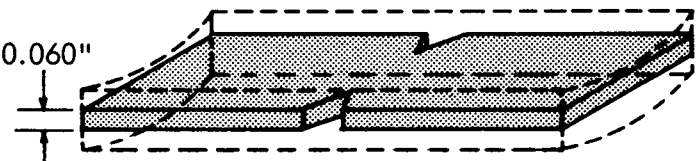
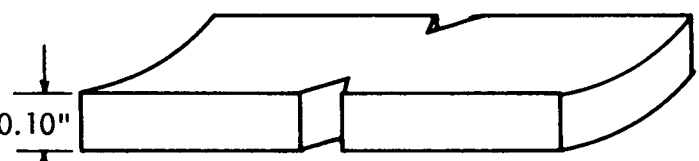
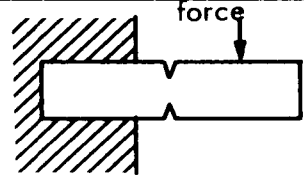
Specimen Type	Geometry	Specimens Used For	Notes
a) Transverse GTA weld in 0.030 in. sheet.	 <p>Notch radius = 0.003"</p> <p>0.040</p> <p>0.040</p> <p>1/2"</p> <p>1"</p> <p>0.145"</p>	1, 3, 10	Specimens post-machine annealed 1 hr. - 982°C (1800°F) prior to fracture and Auger analysis.
b) Surface ground tube wall specimen	 <p>0.060"</p> <p>Other dimensions as for (a) above.</p>	11, 12	
c) Full section tube wall specimen	 <p>0.10"</p> <p>Other dimensions as for (a) above.</p>	11, 12	Fractured and analyzed as-machined.
All specimens fractured at -150°C (-238°F) by impact-type loading as shown.		 <p>force</p>	

FIGURE 4. Geometry of Specimens Used for Auger Spectroscopic Analysis.

in tension while the tube specimens were loaded in such a way that one notch was in tension and the other in compression. Bend radius in all cases was 0.076 cm.(0.030 in.) and the loading rate maintained constant at 2.54 cm./min.(1.0 in./min.).

Scanning Electron Microscopy (SEM)

Examination and characterization of the fracture surfaces of all specimens was accomplished using a Cambridge-Mark IIa scanning electron microscope located at the Westinghouse Research and Development Center. In addition to its basic scanning function this instrument is equipped to provide for energy-dispersive x-ray spectrography as well as for the recording of electron channeling patterns from selected surface areas ($< 5 \mu\text{m}$ in diameter, from a surface layer less than about 30 nm). This instrument therefore provides the unique capability of recording surface features, surface composition and crystallographic details of the exact same area of a specimen. The excellent depth of focus and resolution of the scanning electron microscope eliminates the necessity for specimen preparation, thereby providing for the immediate and direct observation of the fracture surface.

Transmission Electron Microscopy (TEM)

The same half of each fractured specimen which was examined on the scanning electron microscope was used for the transmission electron microscope examinations. Foils were prepared from regions as near to the fracture as possible. Discs 0.32 cm.(0.125 in.) in diameter were punched from foils which had been mechanically ground and polished to about 0.012 cm.(0.005 in.) thickness. These discs were then electropolished at $38^{\circ}\text{C}(100^{\circ}\text{F})$ in an electrolyte consisting of 85 H_2SO_4 -15HF (conc. acids, by volume). Electropolishing was continued until breakthrough occurred. Thin regions adjacent to the breakthrough were examined with 100 kV electrons on a Philips EM-300 electron microscope.

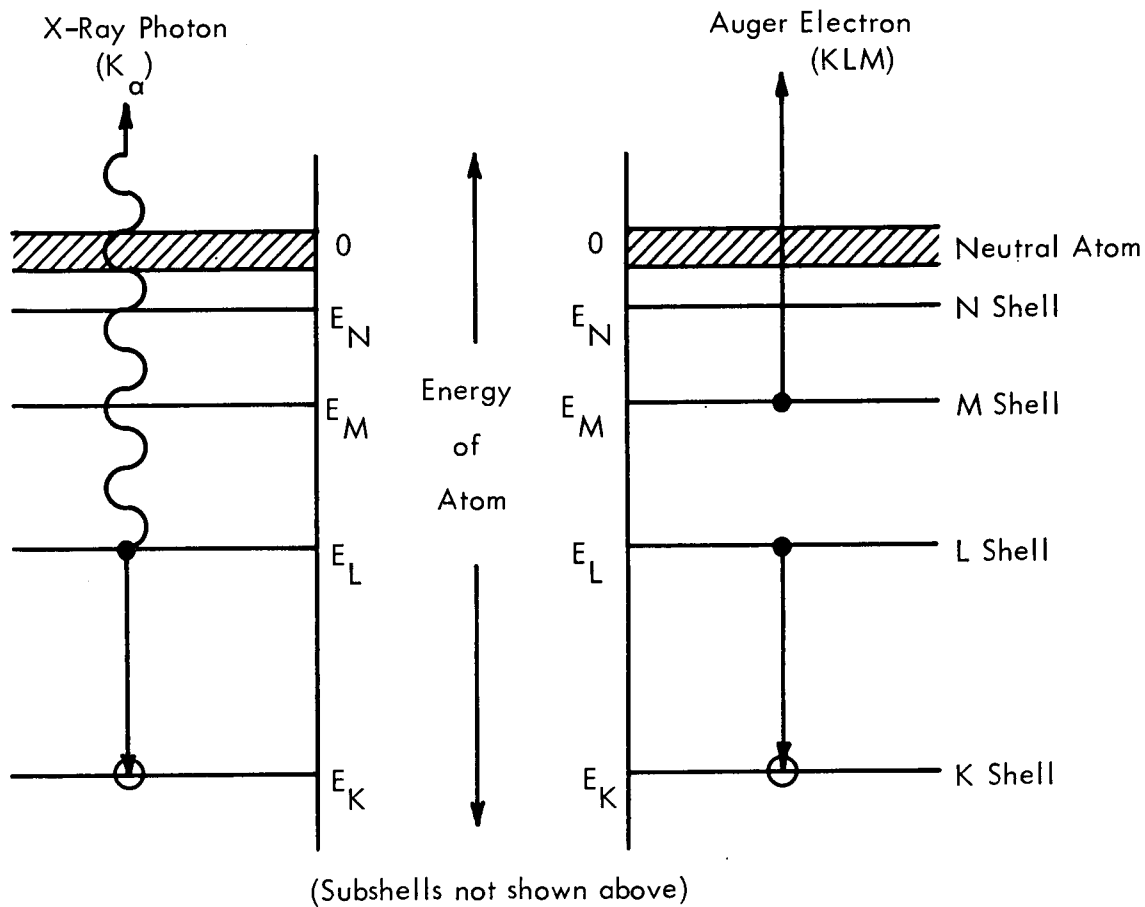
Auger Electron Emission Spectroscopy (AES)

General Description of Technique - Auger electron spectroscopy has developed rapidly over the past several years into a powerful method for the chemical analysis of solid surfaces.

Auger spectroscopy is accomplished by irradiating the surface of a solid with a primary electron beam while energy analysis is performed on the resultant secondary electrons. When this is done peaks are detected in the secondary electron energy distribution function, $N(E)$, when plotted as a function of the energy of the secondary electrons. While the Auger peaks can be detected in the $N(E)$ function directly, they are more evident in the differentiated function, $dN(E)/dE$, due to the fact that differentiation effectively removes the strong background caused by backscattered primary electrons.

The energy of Auger electrons, and hence their position on $dN(E)/dE$ vs. E plots, is directly related to the core levels of the parent atom. Under the excitation of the incident electron beam the atom is ionized; that is, an electron is knocked out of one of the core electron levels. The atom may then decay to the equilibrium state by one of two processes. The first and more familiar way in which this occurs is through the emission of an x-ray, as in the process whereby characteristic x-ray spectra are produced. The other process by which the equilibrium state may be attained is by the emission of an "Auger electron". These two processes are compared diagrammatically in Figure 5 for the case of an atom ionized to the K state. For low electron energies, less than 2 to 3 keV, Auger transitions dominate^(4,5) and they become comparable to x-ray production at 4 keV. If low energy transitions are chosen for study, the Auger technique is very sensitive to all elements except hydrogen and helium which do not possess core electrons.

The energy of the Auger electron produced depends only on the energy levels of the atom and not on the energy of the electron responsible for the initial ionization. Hence, the kinetic energy of the ejected Auger electron may be estimated from a knowledge of the binding energy of the participating core electrons. As the atomic number of the atom increases many more transitions become possible and, lacking well-defined selection rules such as exist for x-ray fluorescence, we are forced to rely on empirical data. Presently this data is supplied by compilation of the Auger spectra of the pure elements. Thus, by analyzing the secondary



X-Ray Process

- a - K electron lost (ionization)
 - b - L electron replaces K electron
 - c - X-Ray photon (K_{α}) emitted
- Normal incident electron beam >30 kV
Typical photon energy produced >4 keV

Auger Process

- a - K electron lost (ionization)
 - b - L electron replaces K electron
 - c - M electron emitted as "Auger electron"
- Normal incident electron beam 2 to 5 kV
Typical Auger electron energy < 2 keV
(Most transitions are of KL_1L_2 , LM_1M_2 , etc. type)

FIGURE 5. Electron Energy Diagram Comparing Transitions Giving Rise to X-Ray and Auger Electron Emissions.

electron energy spectrum of a given specimen, together with the knowledge of the major constituents, we can determine which additional elements are present. The concentration of a particular atomic species can be estimated by comparing its intensity on the experimentally observed Auger spectrum to the intensity of the same peak on the Auger spectrum of the pure element.

The low energy of Auger electrons implies a particularly useful aspect of Auger spectroscopy as an analytical tool. The escape depth of Auger electrons is equal to the electron-electron mean free path in the specimen. Recent measurements indicate this to be < 1 nm for most metals for electron energies < 2 kev. Hence, peaks in the secondary electron energy spectrum which are measured originate from Auger transitions occurring only in the first few atomic layers from the surface. This is of obvious importance in the study of surface- or interface-controlled phenomena. To avoid problems of surface contamination during examination, Auger analysis is normally carried out in systems equipped with sorption pumps for roughing and ion and sublimation pumps for high vacuum. These enable routine operation at pressures in the 10^{-10} torr range. In addition, the composition profile may be determined as a function of depth below the surface by means of an ionized inert gas sputtering attachment.

Details of recent applications of Auger electron spectroscopy to metallurgical studies may be found by reference to the literature⁽⁶⁻¹⁰⁾.

This Program - Specimens representing conditions 1,3,10,11 and 12 (Table 1) were chosen for examination by AES. The analytical work was carried out at Physical Electronics Industries, Edina, Minnesota. Separate specimens - i.e. other than the bend-fractured specimens - were required for these studies due to the fact fracture must be accomplished in situ in the ultra-high vacuum environment of the Auger equipment in order to avoid excessive oxygen and carbon "pick-up" on the fracture surfaces.

Specimens were cooled to approximately -150°C (-238°F) by means of running liquid nitrogen through a copper cooling block used to hold the specimens for fracture. Fracture is achieved by means of an impact-type hammer arrangement, activated externally through a bellows feed-through into the test chamber. Use of a carousel-type specimen holder permitted all specimens to be analyzed in sequence, without the necessity of repeated disruption of the vacuum. To further minimize possible contamination specimens were not fractured until immediately before their respective Auger analyses.

4.0 RESULTS

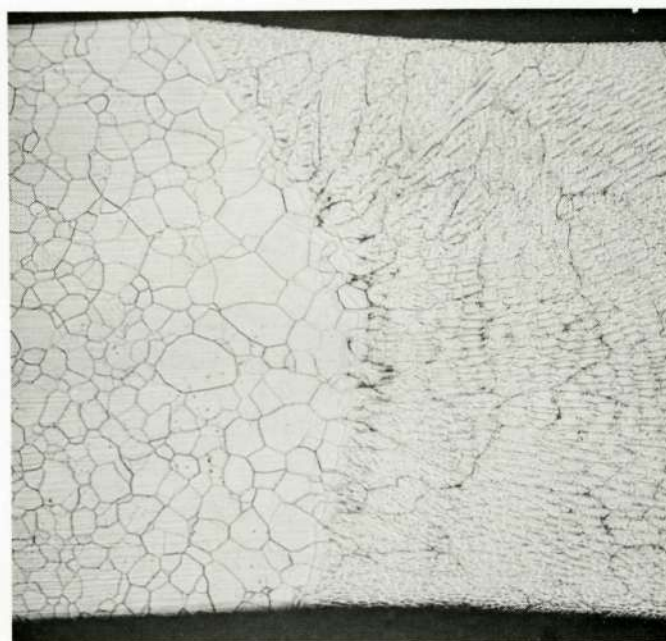
During the course of this investigation it became increasingly probable that the factors responsible for the behavior observed in the aged GTA sheet welds were quite different from those responsible for the low room temperature ductility of the T-111 tube material. The results of the experimental program confirmed this. Hence, the results of the evaluation of these two types of T-111 are considered separately.

4.1 Aged GTA Sheet Welds

Specimen 1. This specimen was aged 1000 hours at 982°C (1800°F) in ultra-high vacuum. The microstructure after aging is shown in Figure 6. Precipitates have developed along the interdendritic boundaries of the weld fusion zone but there is no evidence of grain boundary precipitation. SEM examination of the bend-fractured specimen revealed failure had occurred due to separation along fusion zone grain boundaries, Figure 7. In the 450X micrograph (Figure 7) several of the elongated weld grains are seen to be tipped by regions of ductile rupture. Examination of the specimen fractured in the Auger apparatus indicated failure had occurred largely in the same manner, but isolated regions of cleavage and dimpled rupture were present.

We were unable to obtain a high quality thin foil for examination by transmission electron microscopy from a region in the weld zone near to the fracture. A foil prepared from a region near the fusion zone/ HAZ interface was exceptionally "clean" with no evidence of intragranular precipitation and a low dislocation density.

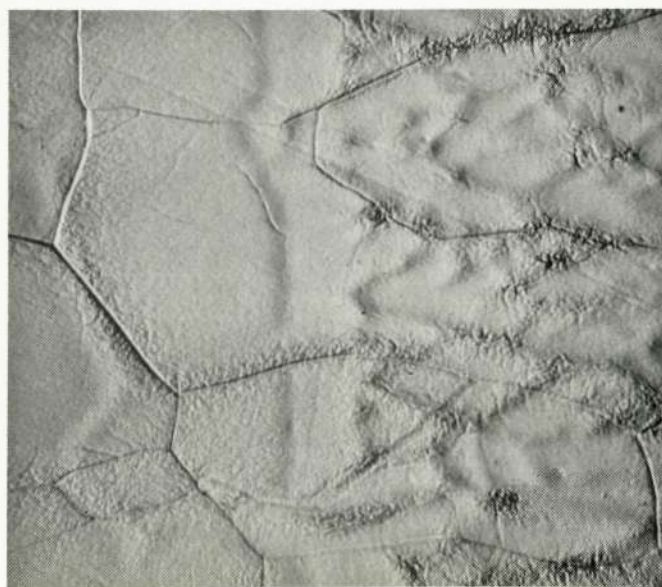
Results of Auger emission spectroscopic analysis performed on a freshly fractured specimen are presented in Table 3. The carbon, oxygen and nitrogen on the fracture surface is mainly the result of gas adsorption rather than segregation of these elements as impurities at the grain boundaries. The second entry for specimen 1, "new area", represents the results obtained by exciting a second area of the fracture surface. The higher C, O and N values are due to the fact this data was accumulated after the fracture surface had been exposed



23,901

HAZ / Weld

80X



23,901

HAZ / Weld

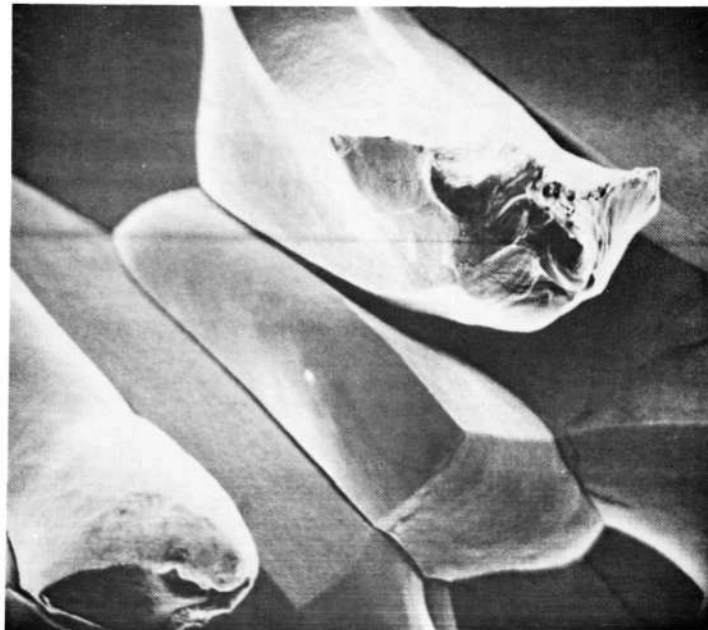
750X

Aged 1000 Hours-982°C(1800°F)

FIGURE 6. Microstructure of GTA Weld Specimen 1.



180X



450X

Aged 1000 Hours-982°C (1800°F)

FIGURE 7. Scanning Electron Micrographs of Fracture Surface of GTA Weld Specimen 1 ; Fractured at -196°C (-320°F).

Table 3. Results of Auger Analyses on GTA Weld Specimens

Specimen	Condition	Concentrations (a/o) ^(a)								
		Ta	Hf	W	C	O	N	F	K	Si
1	As-Fractured	71	7	3.5	5	10	0.5	3	0.3	0
1	New Area	52	5	2.5	14	18	2	1	6.5	0
3	As-Fractured	63	5	3	7	14	1	0.3	0.3	6
3	Sputtered	60	5	3	15	15	1	0.3	1	~0
10	As-Fractured	65	6	3	11	11	1.5	0.3	0.3	1.5

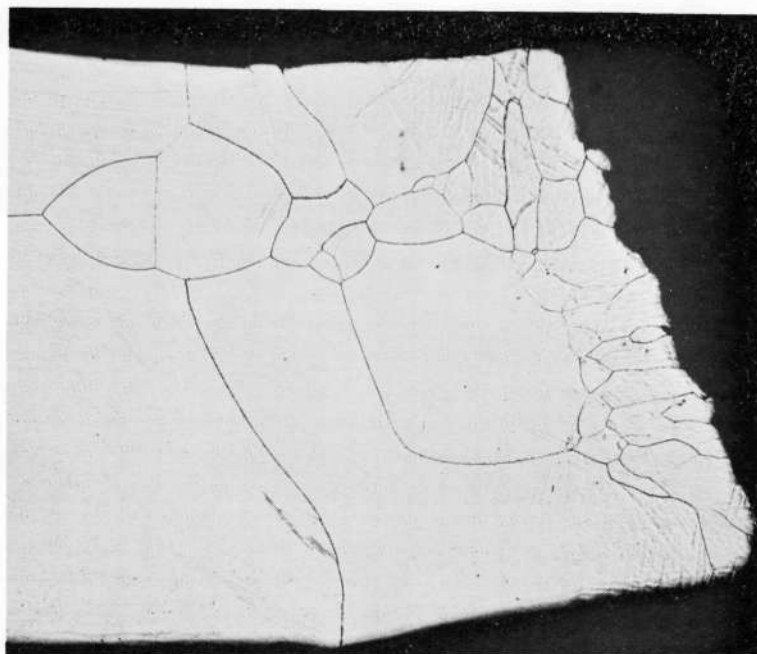
(a) Accuracy of concentrations \pm 20% of recorded values.

for a longer time. Note the hafnium level is much higher and the tungsten level much lower than the nominal alloy composition. This is not at all unusual and confirms earlier results⁽¹⁾. The only significant impurities observed are fluorine and potassium. The actual fluorine concentration may be much higher than recorded on Table 3 since this atom desorbs very rapidly under the electron beam. The magnitude of the potassium peak varied considerably across the fracture surface. While it is not unlikely the fluorine results from pickling and cleaning operations using HF acid, the possible sources of potassium contamination are not so obvious.

Specimen 2. This specimen is identical to specimen 1 (1000 hours-982°C(1800°F)) except for the use of a 1 hour-1982°C(3600°F) post-age anneal. This anneal has resulted in extensive grain growth in the base metal and HAZ, Figure 8. The fusion zone has undergone less significant change. SEM examination of the fracture surface revealed a mixed fracture mode. Regions of the specimen displayed what appeared to be cleavage-type markings while others, apparently differing mainly in orientation, failed by a ductile, dimpled rupture. Micrographs of these various features are shown in Figure 9.

Transmission electron microscopy revealed very little difference between this specimen and specimen 1. Figure 10 is a micrograph of a foil prepared from the weld fusion zone. Some dislocation tangles are in evidence but very little precipitation. Where precipitates were observed they were quite large and blocky and situated at the grain boundaries. Previous extraction and identification of this type of precipitate has shown it to be HfO_2 .

Specimen 3. Aged 5000 hours at 1149°C(2100°F) this specimen shows a microstructure much like that of specimen 1. Precipitation is interdendritic within the weld zone and nil elsewhere, Figure 11. SEM revealed the fracture morphology to be intergranular, the grain boundaries being quite clean and free of precipitation, Figure 12. The specimen fractured for Auger analysis at -150°C(-238°F) also failed by intergranular fracture but, although most grain surfaces were clean, some evidence of coarse precipitation was observed, Figure 13. Analysis of several of the larger precipitates with the energy-dispersive x-ray spectrometer of the scanning microscope showed very high hafnium content. These particles are probably



23,902

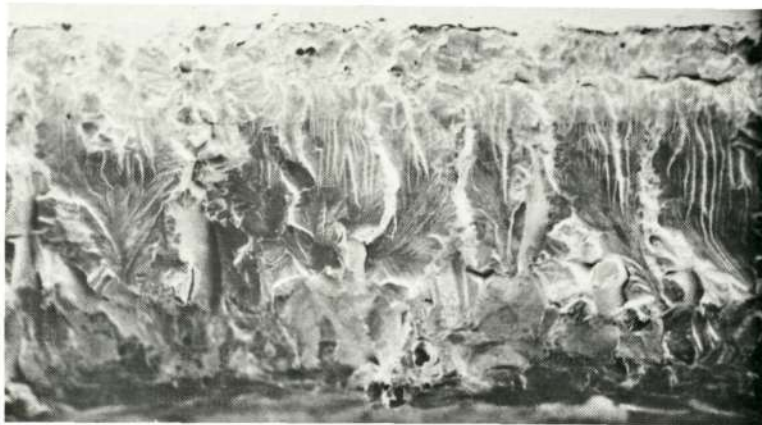
HAZ / Weld

80X

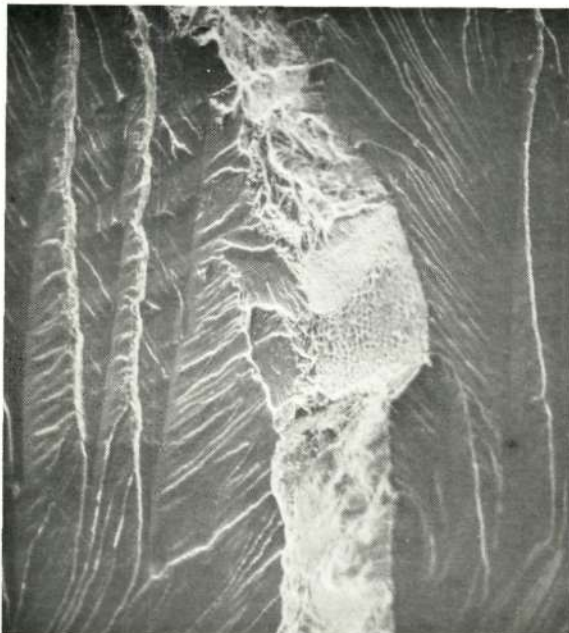
Aged 1000 Hours-982°C(1800°F)
+ 1 Hour - 1982°C (3600°F)

FIGURE 8. Microstructure of GTA Weld Specimen 2.

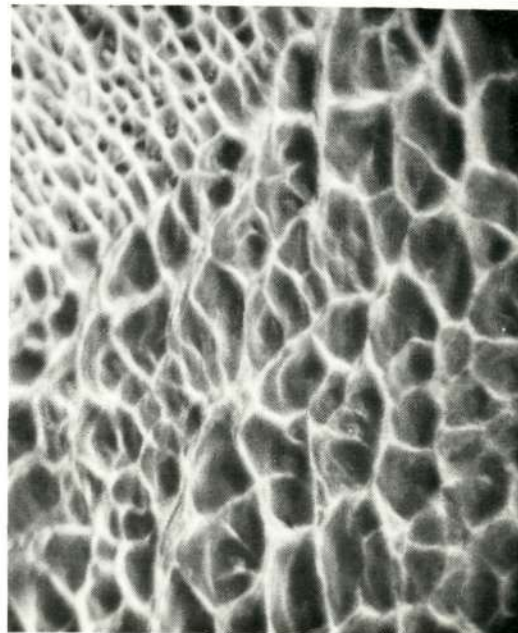
Reproduced from
best available copy.



45X



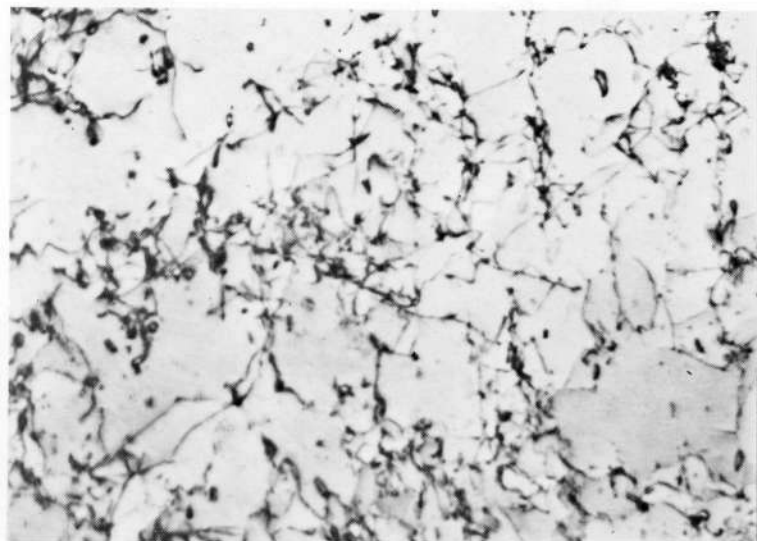
500X



5000X

Aged 1000 Hours - 982°C (1800°F)
+ 1 Hour - 1982°C (3600°F)

FIGURE 9. Scanning Electron Micrographs of Fracture Surface of GTA Weld Specimen 2 ; Fractured at -196°C (-320°F).



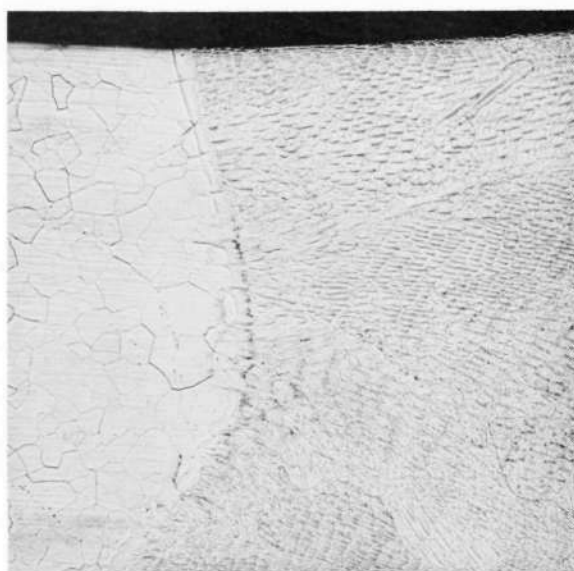
71-3054

0.2μm

76,100X

Aged 1000 Hours - 982°C (1800°F)
+ 1 Hour - 1982°C (3600°F)

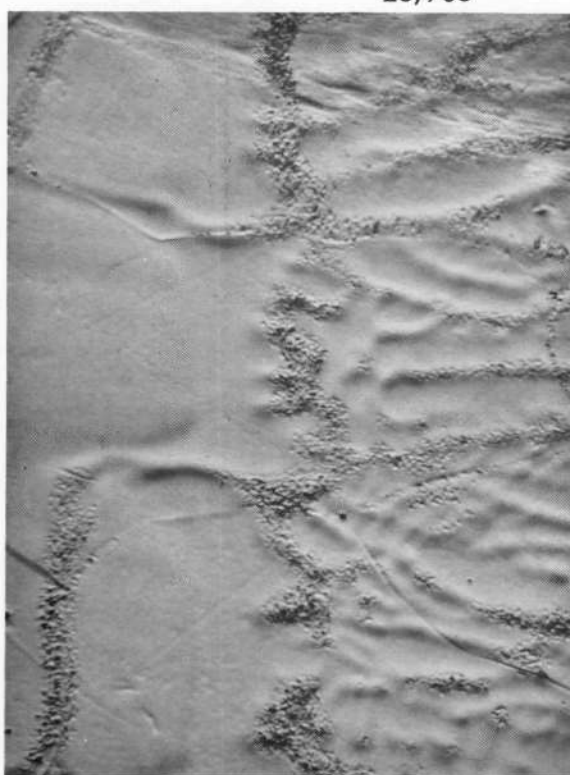
FIGURE 10. Transmission Electron Micrograph of Weld Zone Structure in GTA Weld Specimen 2.



23,903

HAZ/Weld

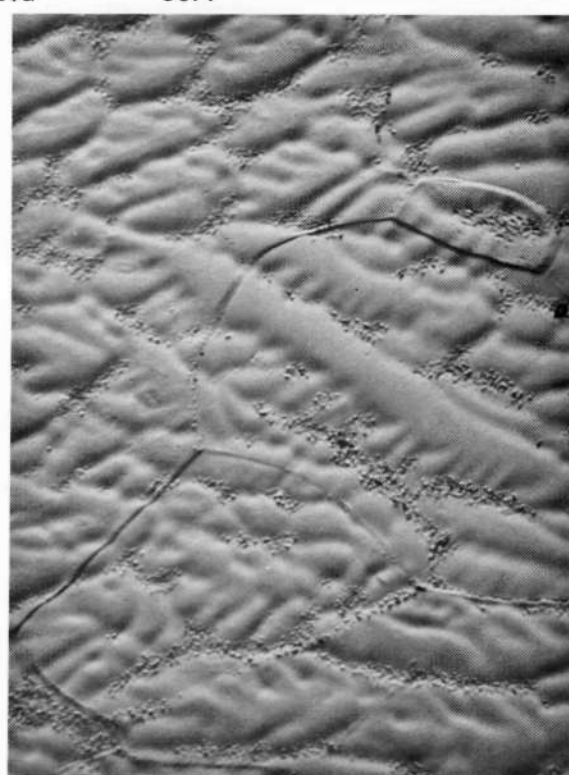
80X



23,903

HAZ/Weld

750X



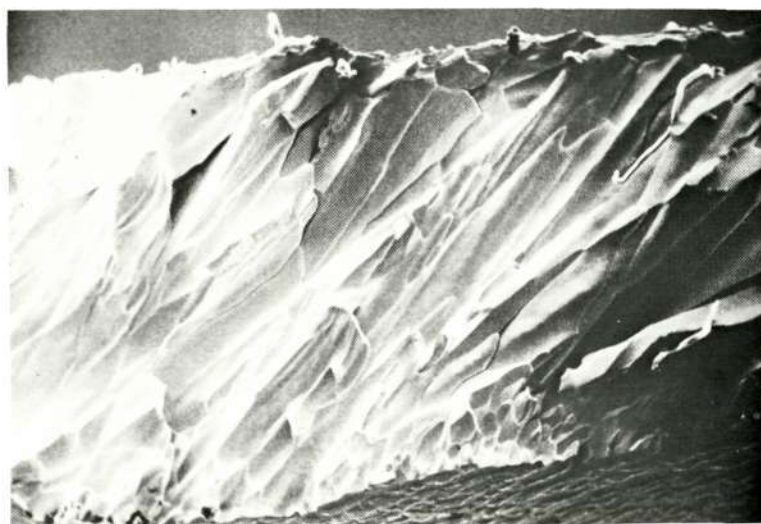
23,903

Weld

750X

Aged 5000 Hours - 1149°C (2100°F)

FIGURE 11. Microstructure of GTA Weld Specimen 3.



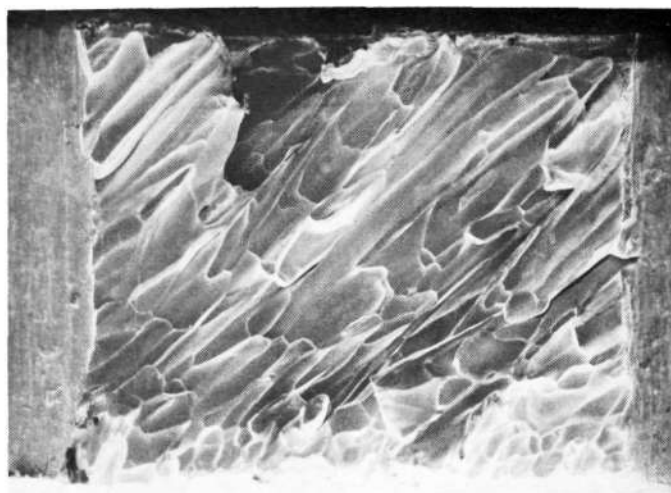
45X



450X

Aged 5000 Hours - 1149°C (2100°F)

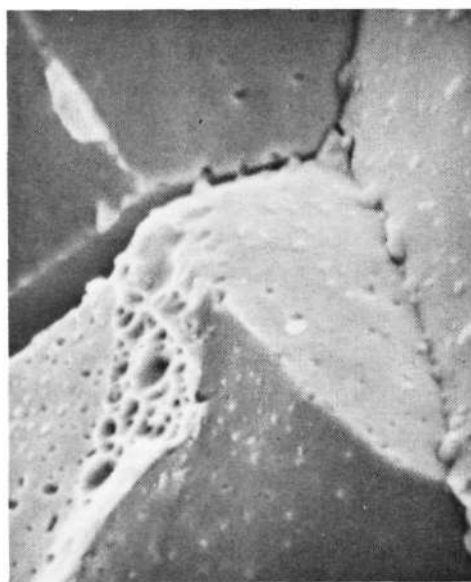
FIGURE 12. Scanning Electron Micrographs of Fracture Surface of GTA Weld Specimen 3 ; Fractured at -196°C (-320°F).



45X



4500X



4500X

Aged 5000 Hours - 1149°C (2100°F)

FIGURE 13. Scanning Electron Micrographs of Fracture Surface of GTA Weld Specimen 3 ; Fractured in Auger Apparatus at -150°C (-238°F).

HfO₂. Unfortunately, we were not able to obtain a satisfactory foil for TEM examination of this specimen.

Results of Auger analysis on specimen 3 are shown in Table 3. As mentioned previously for specimen 1, the carbon, oxygen and nitrogen concentrations are due to adsorption in the high vacuum environment following fracture. As for specimen 1 we again have fluorine and potassium present at the grain boundaries. Unlike specimen 1 we also have a considerable silicon concentration, 6%. The second entry, "sputtered", in Table 3 is the result obtained when the fracture surface was argon sputtered to remove about 1 nm (10 Å). The silicon concentration is now zero. Position of the silicon peak on the Auger spectrum is known to be noticeably altered if the silicon is present as SiO₂ rather than elemental silicon. From the observed silicon peak on the Auger spectrum of specimen 3 we can conclude with reasonable certainty that a very thin layer, perhaps only a monolayer, of silicon was present at the fusion zone grain boundaries.

Specimen 4. The microstructure of this specimen, aged 10,000 hours at 1149°C(2100°F), is shown in Figure 14. The additional 5000 hour aging has not altered this appreciably from that of specimen 3 (Figure 11). Totally unexpected therefore was the ductile behavior of this specimen in bending at -196°C(-320°F). To completely fracture this specimen it had to be bent back and forth a number of times. Scanning micrographs of the fracture are shown in Figure 15. Regions of dimpled rupture quite often showed precipitate-void relationships such as seen in the 4500X micrograph of Figure 15.

Examination of this specimen by transmission electron microscopy revealed nothing unusual except for a rather large concentration of grain boundary oxide precipitates, in many cases quite coarse. This is in agreement with the SEM observations on the fracture surface.

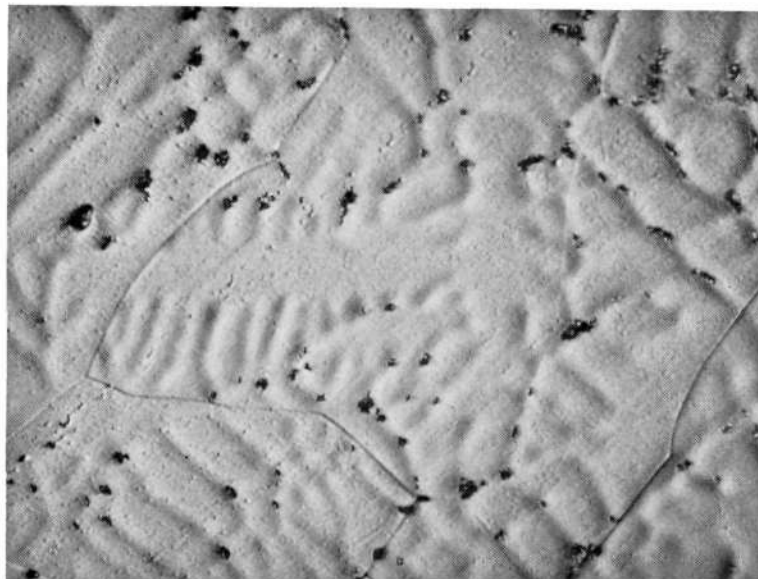
Specimen 5. This specimen was aged 10,000 hours at 1149°C(2100°F) and given a 1 hour-1982°C(3600°F) post-age anneal. The microstructure of the specimen bend-fractured at -196°C(-320°F), Figure 16, showed some evidence of deformation twinning in the fusion



23,904

HAZ / Weld

750X



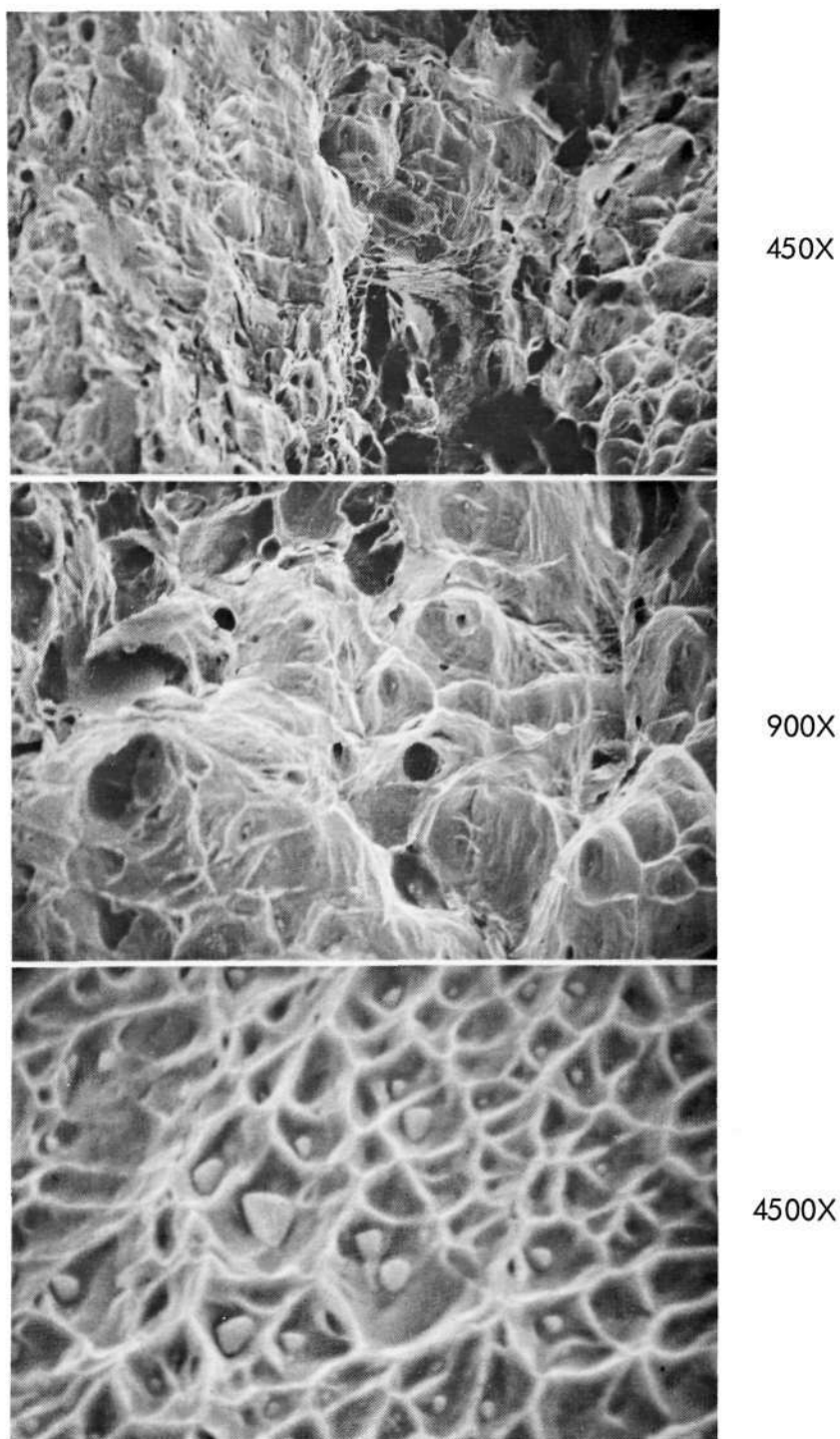
23,904

Weld

750X

Aged 10,000 Hours-1149°C (2100°F)

FIGURE 14. Microstructure of GTA Weld Specimen 4.



Aged 10,000 Hours - 1149°C (2100°F)

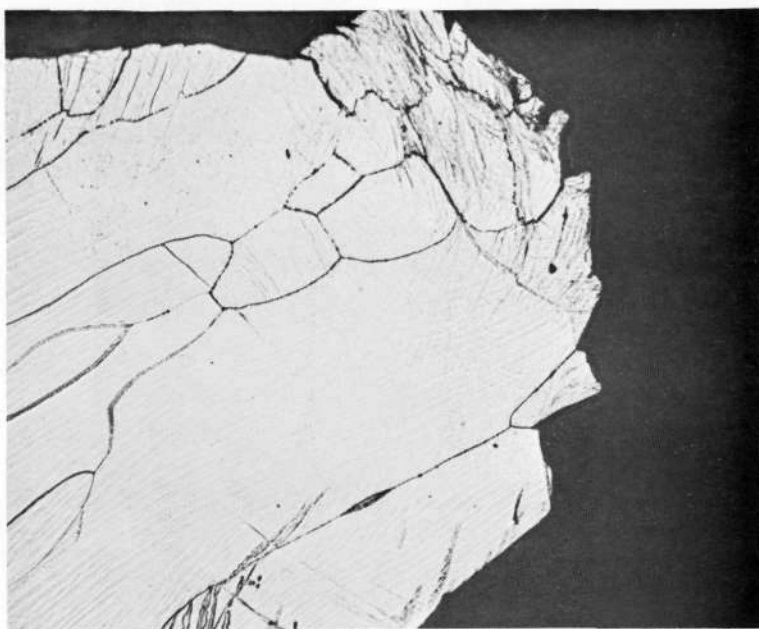
FIGURE 15. Scanning Electron Micrographs of Fracture Surface of GTA Weld Specimen 4 ; Fractured at -196°C (-320°F).



23,905

HAZ / Weld

80X



23,905

Fracture

80X

Aged 10,000 Hours-1149°C (2100°F)
+ 1 Hour - 1982°C (3600°F)

FIGURE 16. Microstructure of GTA Weld Specimen 5.

zone. The fracture appears to have occurred by more than one process. SEM examination confirmed the mixed fracture mode, Figure 17. Fracture has been the result of cleavage and ductile rupture. Most of the regions of ductile rupture were characterized by a high concentration of precipitates within the dimpled pockets. Note the similarity between this specimen and specimen 2 (Figure 9) which was also given a $1982^{\circ}\text{C}(3600^{\circ}\text{F})$ post-age anneal.

TEM examination showed the fusion zone grain volumes to be relatively clean. Precipitates that were present were generally located along the grain boundaries. Most dislocations observed were found to lie along one or two directions, Figure 18. Observations of dislocation-precipitate interactions were rare, due at least in part to the scarcity of precipitation.

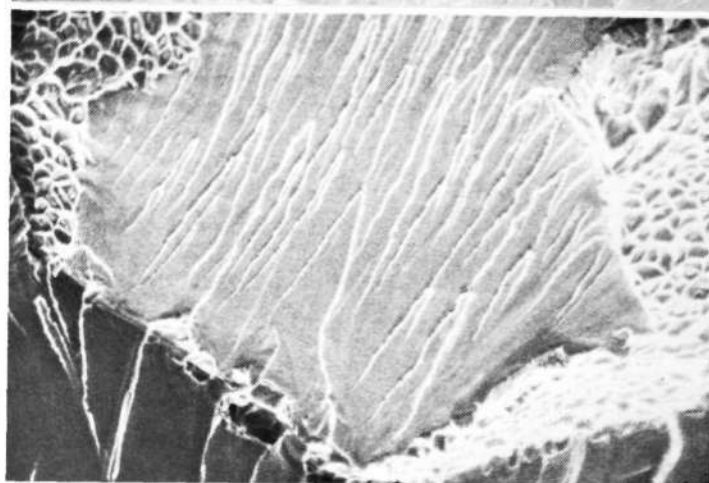
Specimen 6. Aged 10,000 hours at $1316^{\circ}\text{C}(2400^{\circ}\text{F})$, the microstructure of this specimen showed an increase in the amount of grain boundary precipitation in the heat affected zone and a decrease in the interdendritic precipitate in the fusion zone, Figure 19. Scanning micrographs of the bend-fractured specimen reveal regions of dimpled rupture together with cleavage failure, Figure 20. Certain similarities can be noted between the fracture behavior of specimen 6 and specimens 2 (Figure 9) and 5(Figure 17).

The dislocation density was generally low with some evidence of cross-slip and dipole formation, Figure 21. Typically, evidence of precipitation was scarce except for oxide particles at the grain boundaries.

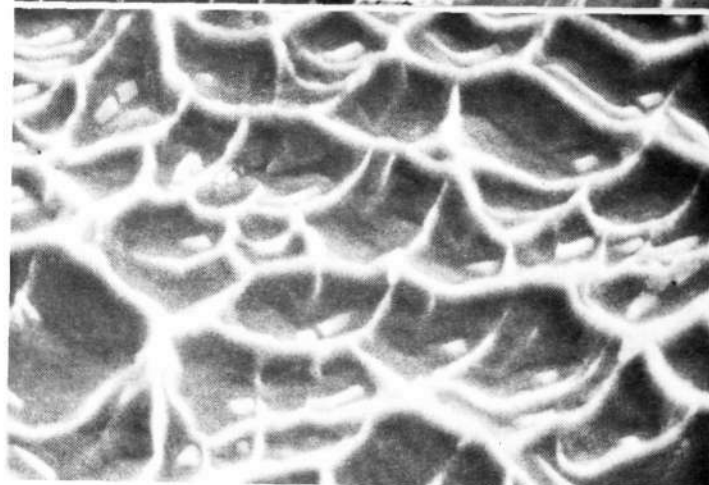
Specimen 7. This specimen was given a 1 hour- $1982^{\circ}\text{C}(3600^{\circ}\text{F})$ anneal after aging for 10,000 hours at $1316^{\circ}\text{C}(2400^{\circ}\text{F})$. Little evidence of the prior weld structure remains in the fusion zone, Figure 22, and the grain boundary regions exhibit a peculiar broadening effect. Fracture morphology is mixed with regions of dimpled rupture and cleavage, Figure 23. Precipitates are associated with most of the regions of ductile rupture. TEM on this specimen indicated a structure much like that of specimen 6, with precipitates being found only at or very near the grain boundaries.



160X



800X



4000X

Aged 10,000 Hrs. -1149°C (2100°F) + 1 Hour -1982°C (3600°F)

FIGURE 17. Scanning Electron Micrographs of Fracture Surface of GTA Weld Specimen 5 ; Fractured at -196°C (-320°F).



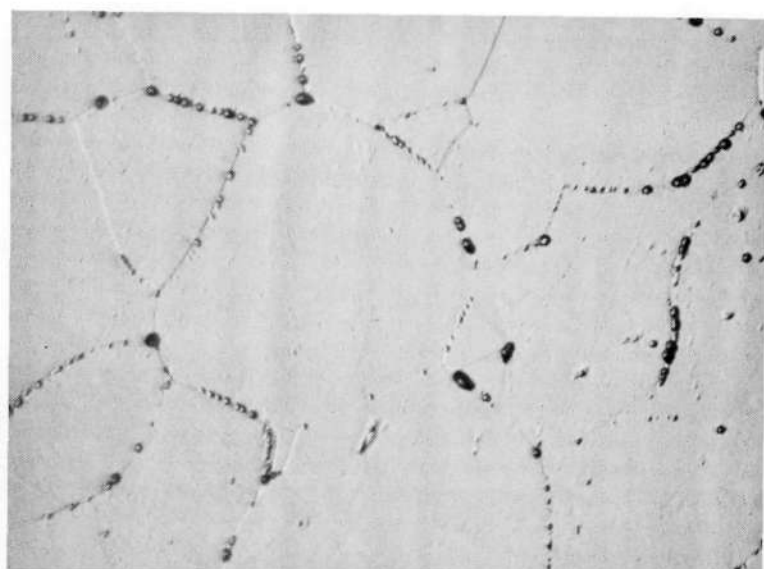
71-2936

0.5 μm

39,220X

Aged 10,000 Hours - 1149°C (2100°F)
+ 1 Hour - 1982°C (3600°F)

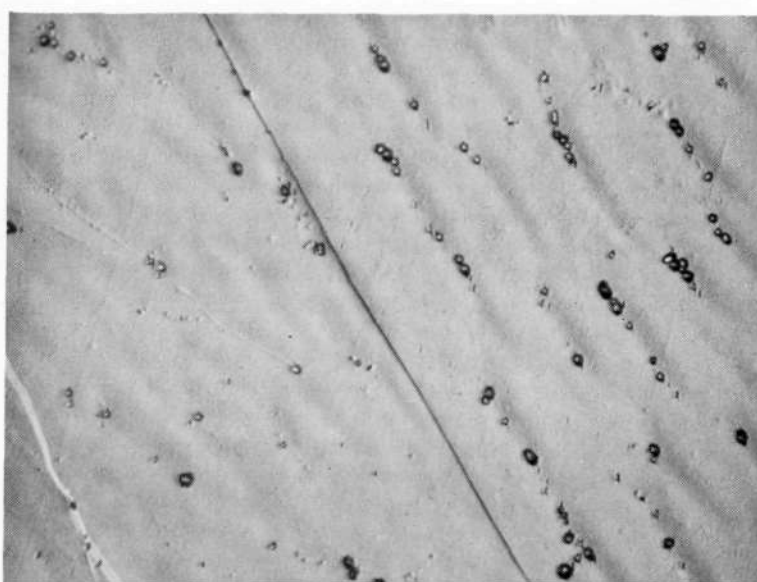
FIGURE 18. Transmission Electron Micrograph of GTA Weld Specimen 5.



23,906

HAZ

750X



23,906

Weld

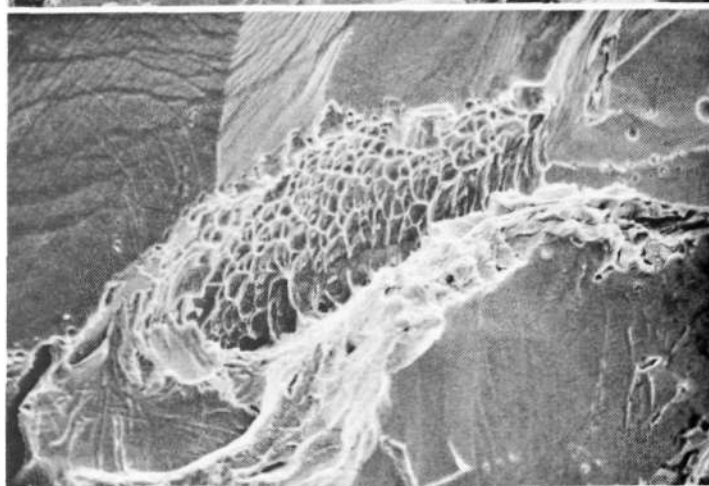
750X

Aged 10,000 Hours-1316°C (2400°F)

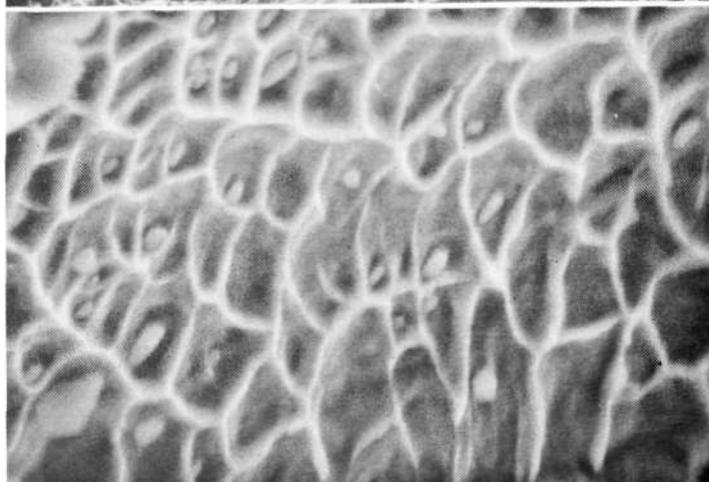
FIGURE 19. Microstructure of GTA Weld Specimen 6.



110X



1100X

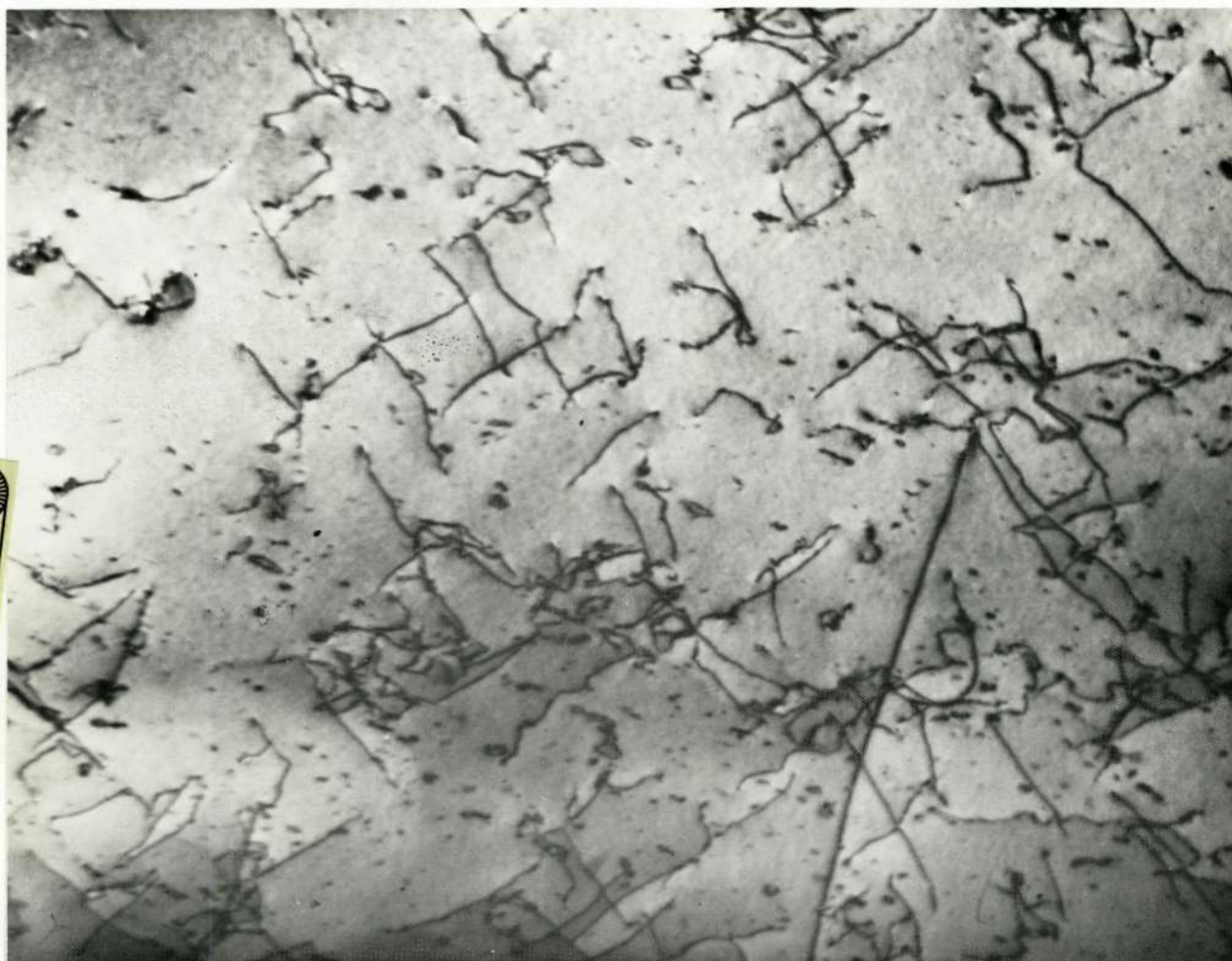


5500X

Aged 10,000 Hours - 1316°C (2400°F)

FIGURE 20. Scanning Electron Micrographs of Fracture Surface of GTA Weld Specimen 6 ; Fractured at -196°C (-320°F).

Reproduced from
best available copy.



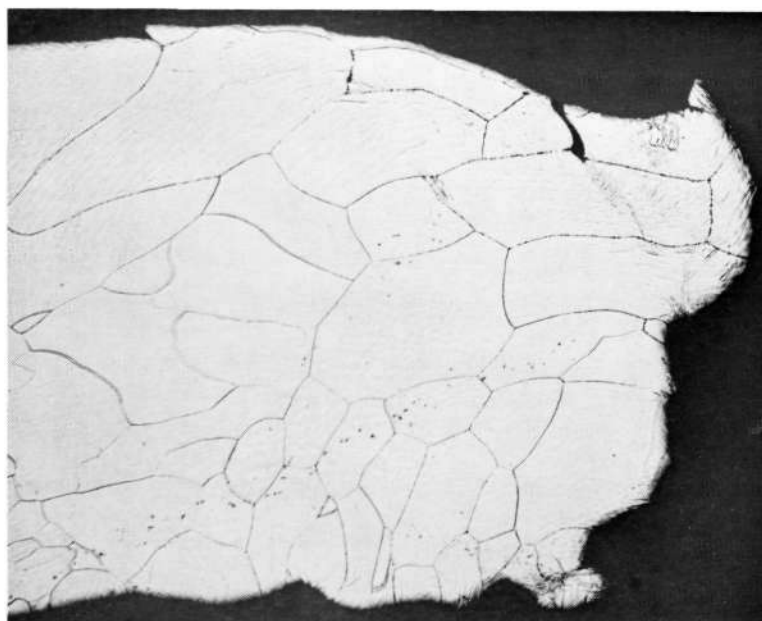
71-2955

0.2 μm

126,600X

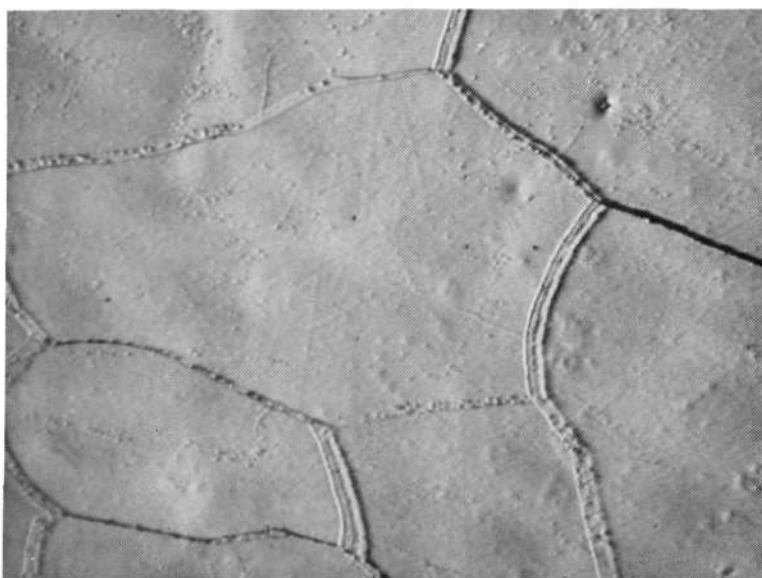
Aged 10,000 Hours - 1316°C (2400°F)

FIGURE 21. Transmission Electron Micrograph of GTA Weld Specimen 6.



23,907

80X

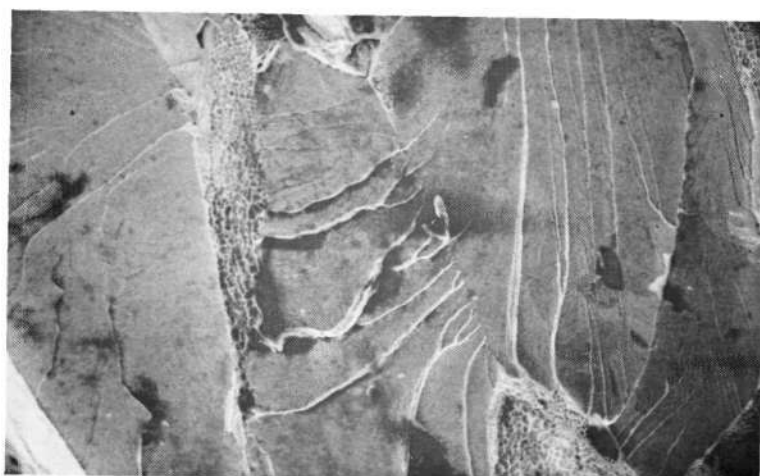


23,907

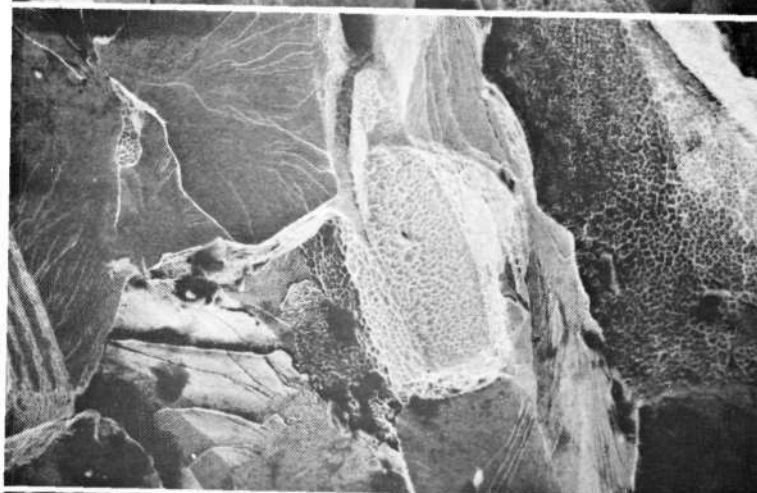
750X

Aged 10,000 Hours - 1316°C (2400°F)
+ 1 Hour - 1982°C (3600°F)

FIGURE 22. Microstructure of GTA Weld Specimen 7.



200X



200X



2000X

Aged 10,000 Hours- 1316°C (2400°F) + 1 Hour- 1982°C (3600°F)

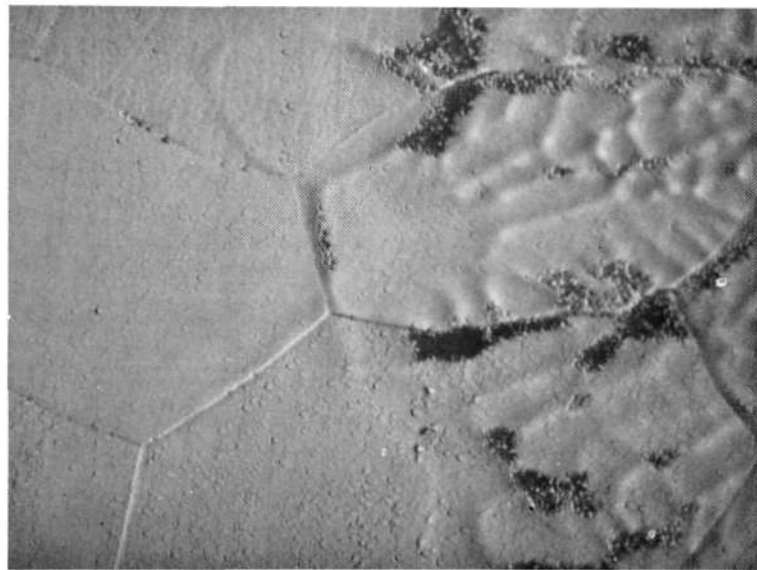
FIGURE 23. Scanning Electron Micrographs of Fracture Surface of GTA Weld Specimen 7 ; Fractured at -196°C (-320°F).

Specimen 8. This specimen was aged 1000 hours at 1149°C (2100°F). The microstructure is similar to that observed previously (specimen 3) after aging at that temperature. Precipitation is occurring interdendritically in the weld fusion zone but virtually nowhere else, Figure 24. SEM examination of the bend-fractured specimen, Figure 25, revealed regions of ductile failure, intergranular fracture and cleavage. Preference for one mode of failure over the others appeared to depend on the orientation of the grain structure with respect to the bending plane. A good foil was not obtained from the weld zone for transmission electron microscopy. A foil prepared from base metal revealed only the presence of isolated grain boundary precipitates.

Specimen 9. This specimen was aged 1000 hours at 1149°C (2100°F) and given a 1 hour post-age anneal at 1982°C (3600°F). The high temperature anneal has reduced the evidence of interdendritic precipitation in the fusion zone, Figure 26. The section in Figure 26 showing the fracture indicates considerable deformation occurred prior to failure. Scanning micrographs of the bend-fractured specimen are similar to those of the other specimens given the 1982°C (3600°F) post-age anneal. Regions of cleavage and dimpled fracture are intermixed, Figure 27, with precipitates typically associated with the ductile regions.

Transmission electron microscopy revealed the matrix to have an exceptionally low dislocation density, presumably due to the "cleaning-up" effect of the high temperature post-age anneal. The general matrix condition can be seen by reference to Figure 28 where we observe dislocation interactions with some of the few intragranular precipitates present. Figure 29 shows two micrographs of HfO_2 particles along a grain boundary in the weld fusion zone. Note the near total absence of dislocations in the vicinity of the boundary.

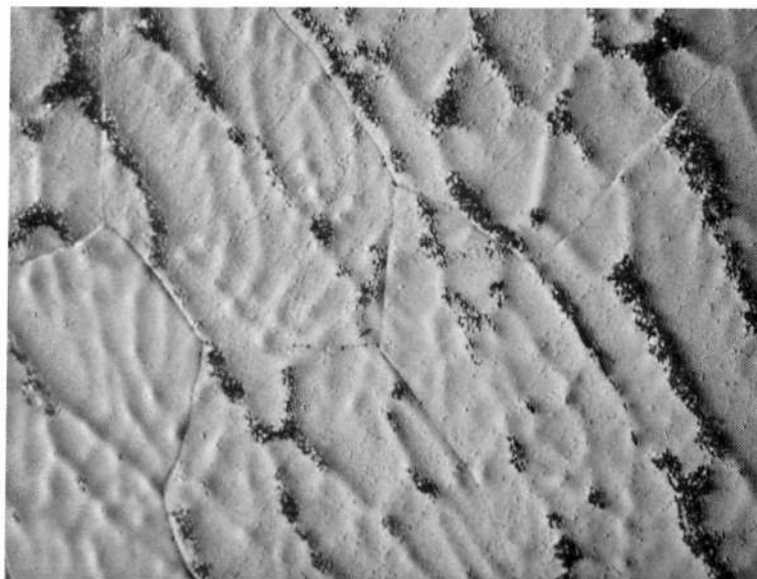
Specimen 10. This specimen differed from all the other GTA weld specimens in that it was given a 1 hour- 1982°C (3600°F) post-weld anneal prior to aging 1000 hours at 1149°C (2100°F). All previous specimens had been given the "standard" 1 hour- 1316°C (2400°F) post-weld anneal. The microstructure of this specimen is shown in Figure 30 where the coarse grain size resulting from the high temperature anneal is apparent.



23,908

HAZ / Weld

750X



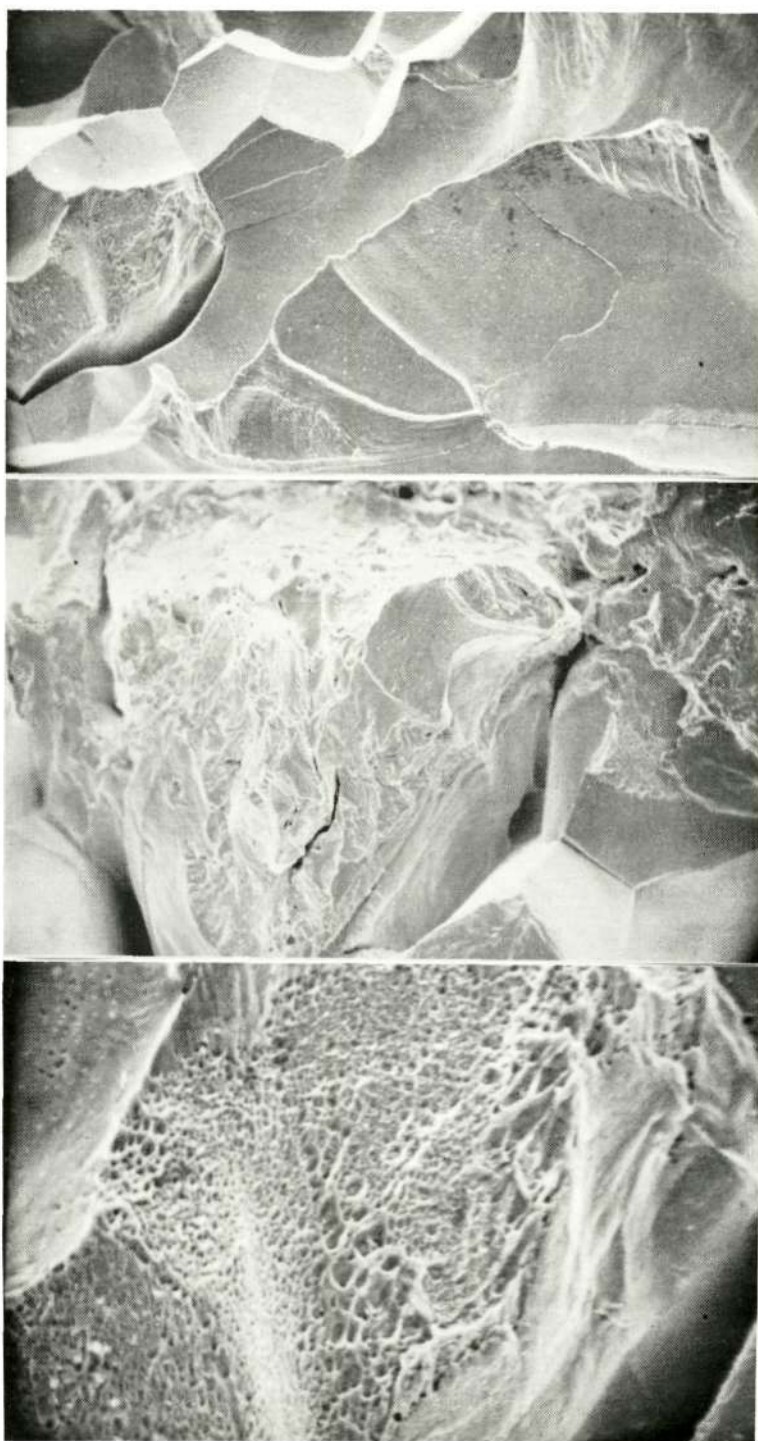
23,908

Weld

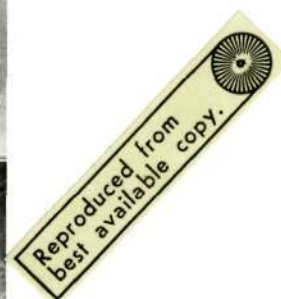
750X

Aged 1000 Hours - 1149°C (2100°F)

FIGURE 24. Microstructure of GTA Weld Specimen 8.



450X

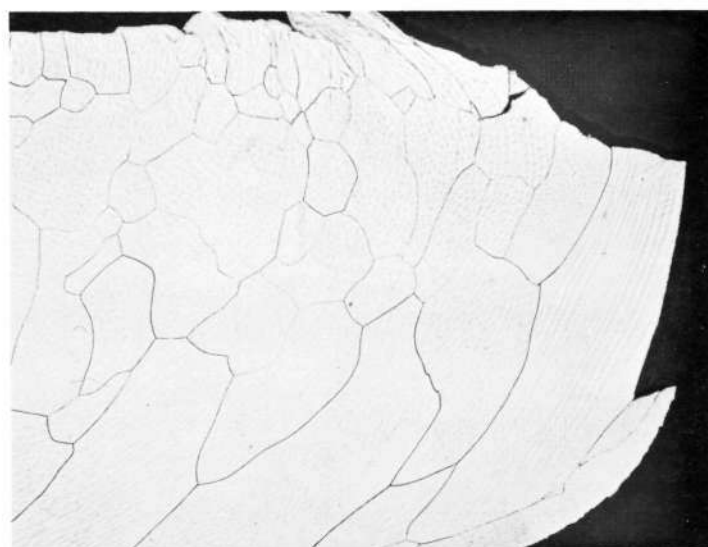


450X

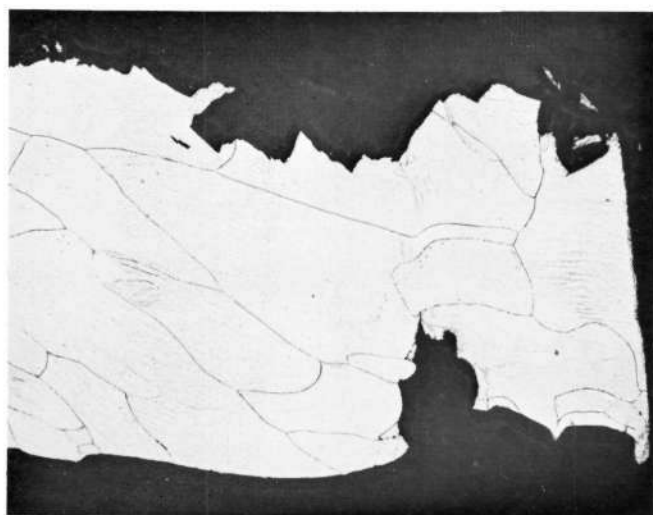
2000X

Aged 1000 Hours - 1149°C (2100°F)

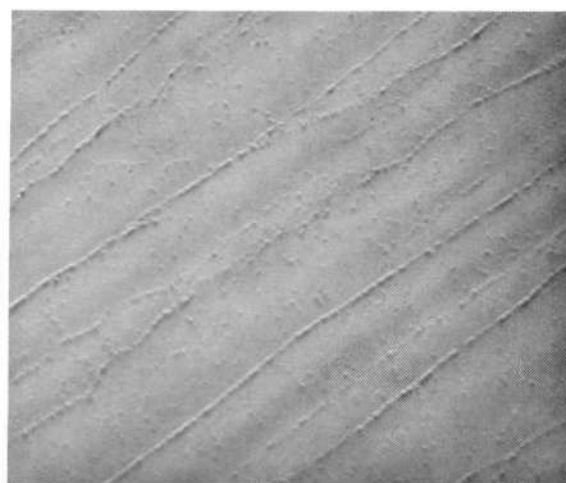
FIGURE 25. Scanning Electron Micrographs of Fracture Surface of GTA Weld Specimen 8 ; Fractured at -196°C (-320°F).



23,909 Longitudinal Section 80X



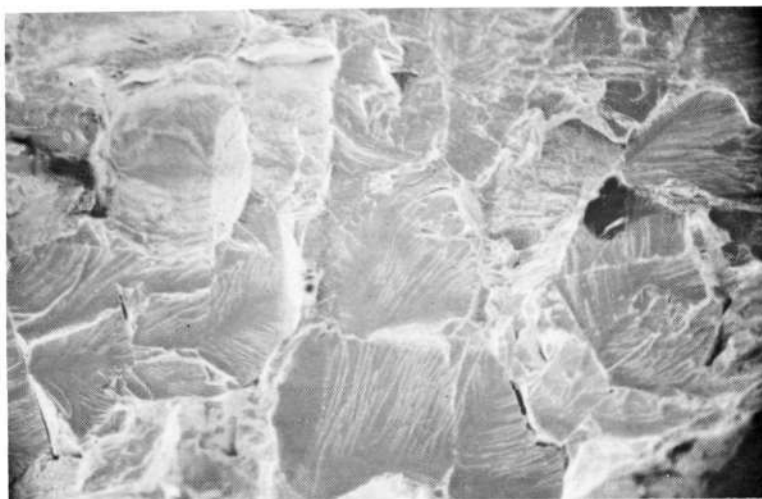
23,909 Transverse Section 80X



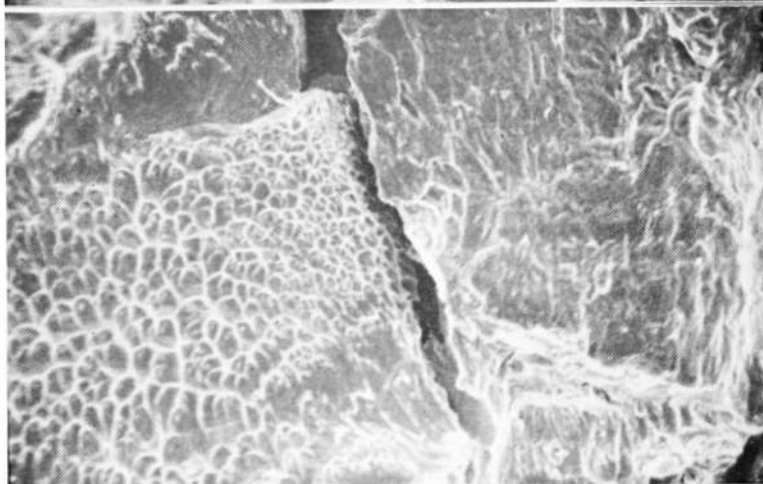
23,909 Weld 750X

Aged 1000 Hours - 1149°C (2100°F)
+ 1 Hour - 1982°C (3600°F)

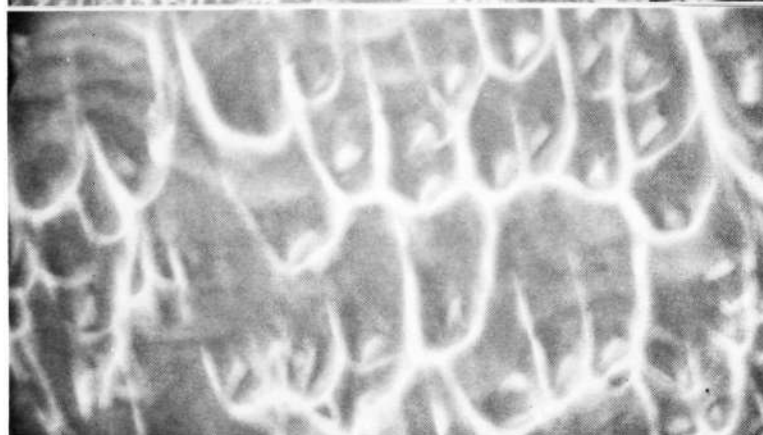
FIGURE 26. Microstructure of GTA Weld Specimen 9.



180X



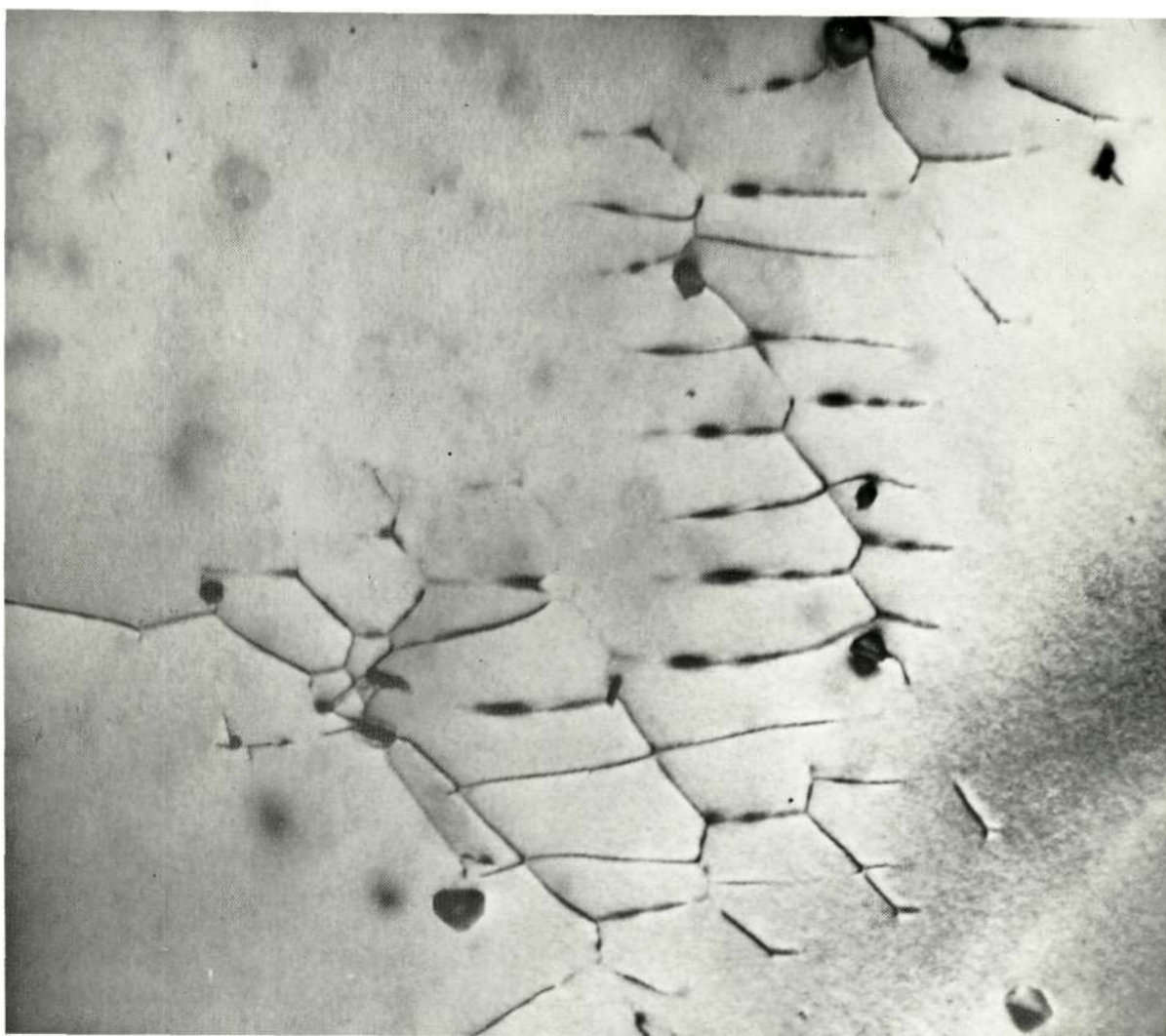
800X



4000X

Aged 1000 Hours - 1149°C (2100°F) + 1 Hour -1982°C (3600°F)

FIGURE 27. Scanning Electron Micrographs of Fracture Surface of GTA Weld Specimen 9 ; Fractured at -196°C (-320°F).



Reproduced from
best available copy.

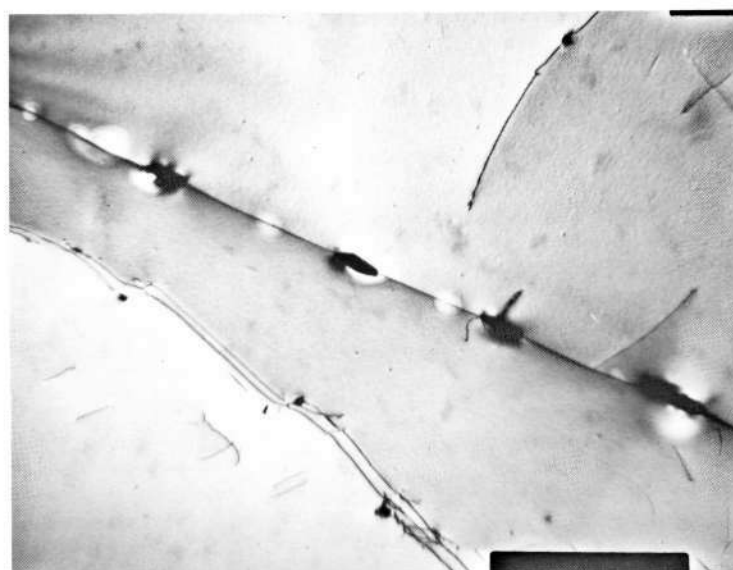
72-0009

0.4 μm

57,800X

Aged 1000 Hours-1149°C (2100°F)
+ 1 Hour-1982°C (3600°F)

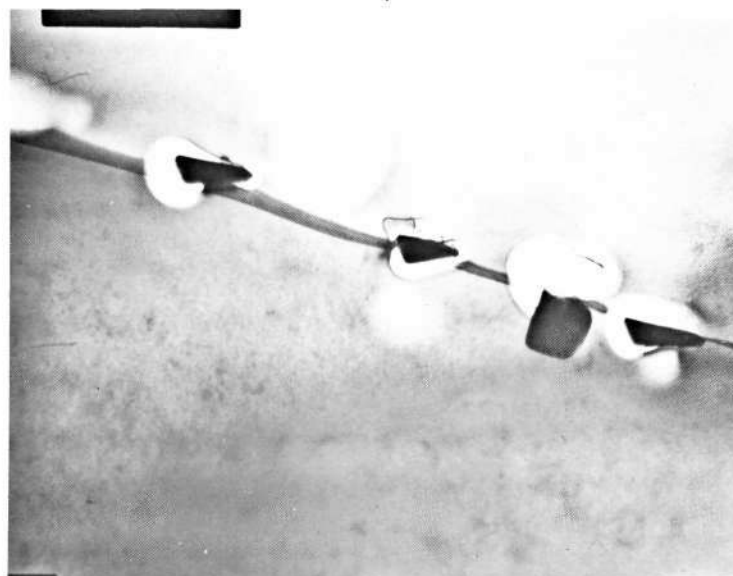
FIGURE 28. Transmission Electron Micrograph of GTA
Weld Specimen 9.



72-0007

2.0 μm

9500X



72-0001

0.5 μm

28,900X

Aged 1000 Hours - 1149°C (2100°F)
+ 1 Hour - 1982°C (3600°F)

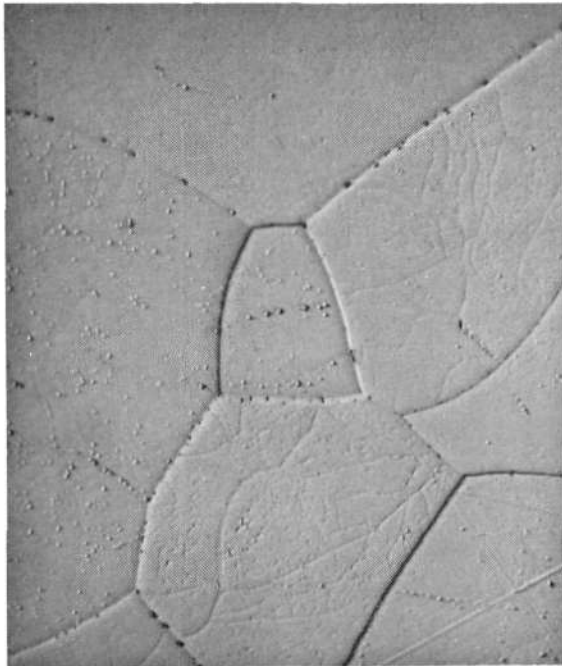
FIGURE 29. Transmission Electron Micrographs of GTA Weld Specimen 9.



23,910

HAZ/Weld

100X



23,910

" Weld "

750X



23,910

Base Metal

750X

Post-Weld Annealed 1 Hour - 1982°C (3600°F)
 + Aged 1000 Hours - 1149°C (2100°F)

FIGURE 30. Microstructure of GTA Weld Specimen 10.

Scanning micrographs of the fracture surfaces of the bend-fractured specimen and the Auger-fractured specimen are presented in Figures 31 and 32, respectively. Both specimens display predominantly intergranular fracture although the Auger specimen, tested at a slightly higher temperature, does exhibit regions of dimpled rupture, usually associated with areas of high grain boundary precipitate density.

A transmission micrograph of a region within the fusion zone and very near the fracture is shown in Figure 33. The sub-boundaries present were probably formed by dislocation rearrangements occurring during the post-weld anneal while the tangles of matrix dislocations more likely occurred during bend-fracturing. At lower magnifications it appeared as if dislocation-precipitate interactions were responsible for the tangles seen; however, examination at higher magnifications established the lack of matrix precipitation.

Results of Auger analysis of this specimen are presented in Table 3. Similar to the results on specimen 3, fluorine, potassium and silicon were found on the fracture surface. One possible reason the silicon concentration was lower than for specimen 3 is the fact the failure did not occur solely by intergranular fracture. Sputtering (data not given in Table 3) of only 0.6 nm (6 \AA) from the fracture surface was sufficient to remove the silicon peak from the Auger spectrum.

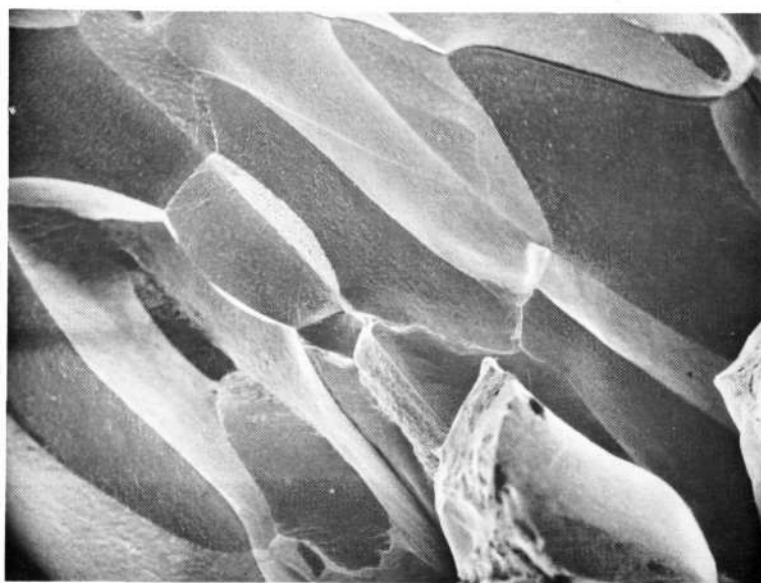
4.2 Aged T-111 Tubing

Specimen 11. The microstructure of this material, aged for 7500 hours at 1038°C (1900°F) is shown in Figure 34. Experience with T-111 has established that the grain boundary precipitate observed is almost certainly HfO_2 . The plentiful occurrence of this precipitate implies a much higher oxygen content than normal for this alloy.

Scanning micrographs of the fracture surface of the specimen bend-fractured at -196°C (-320°F) are shown in Figure 35. The fracture is $>90\%$ intergranular with isolated regions of



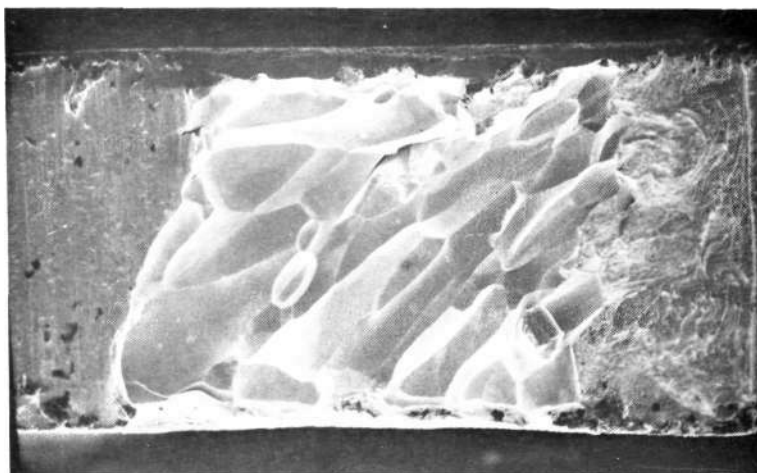
45X



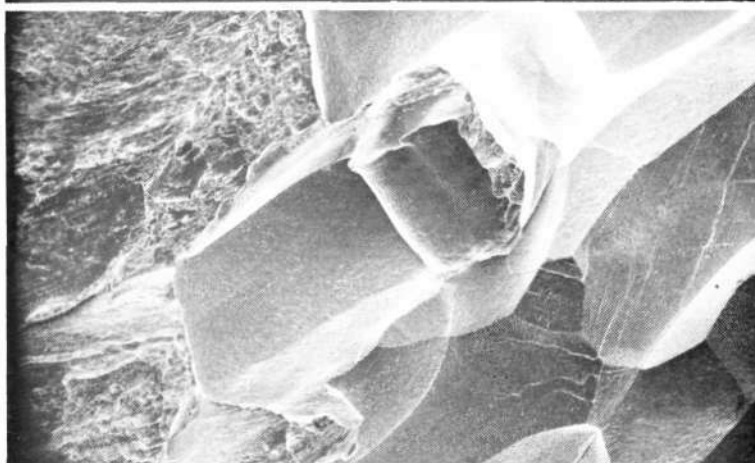
180X

Post-Weld Annealed 1 Hr. -1982°C (3600°F)
 + Aged 1000 Hours -1149°C (2100°F)

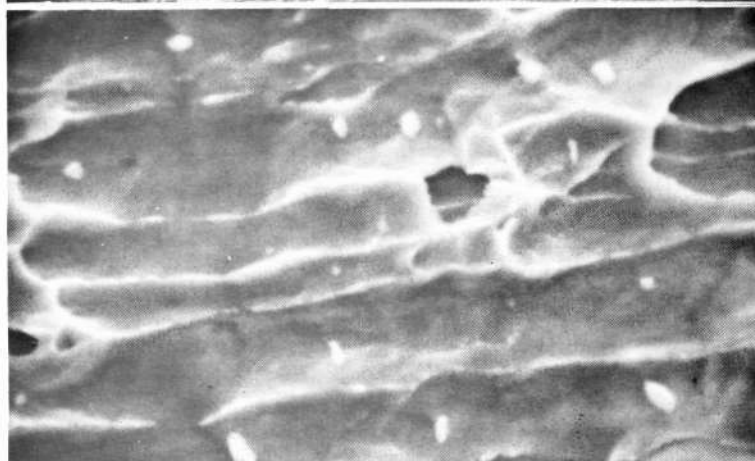
FIGURE 31. Scanning Electron Micrographs of Fracture Surface of GTA Weld Specimen 10 ; Fractured at -196°C (-320°F).



45X



180X



8500X

Post-Weld Annealed 1 Hour -1982°C (3600°F)
+ Aged 1000 Hours -1149°C (2100°F)

FIGURE 32. Scanning Electron Micrographs of Fracture Surface of GTA Weld Specimen 10; Fractured in Auger Apparatus at -150°C (-238°F).



72-0018

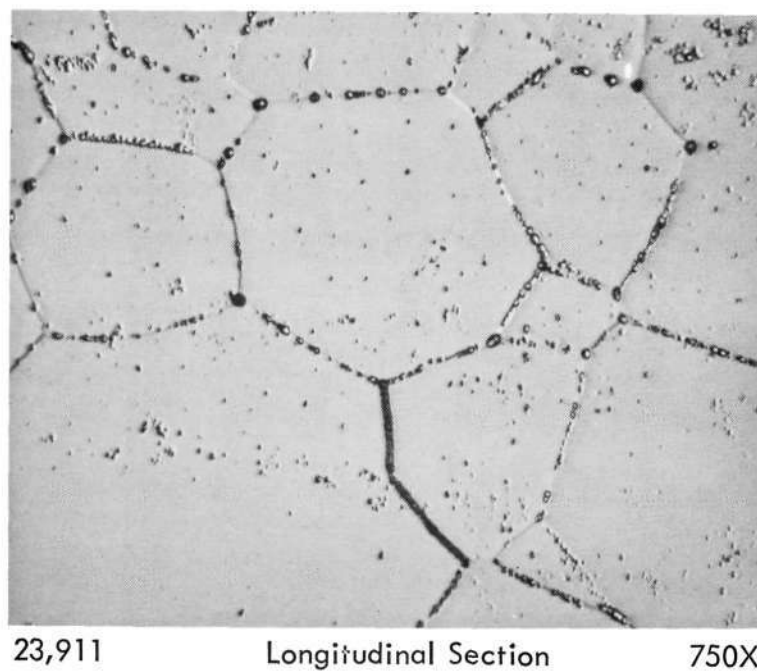
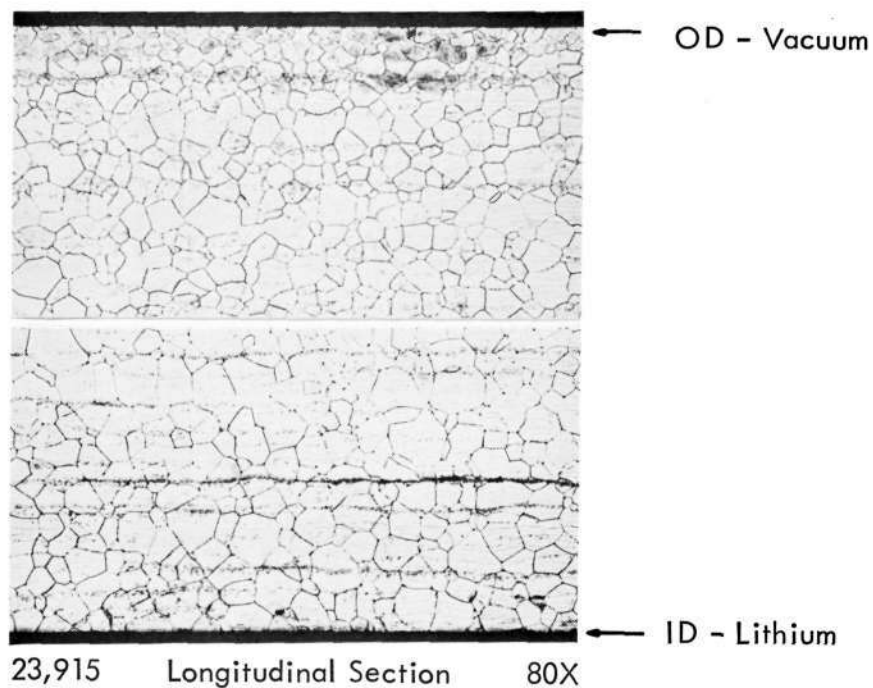
0.3 μm

62,400X

Post-Weld Annealed 1 Hr.-1982°C (3600°F)
+ Aged 1000 Hours-1149°C (2100°F)

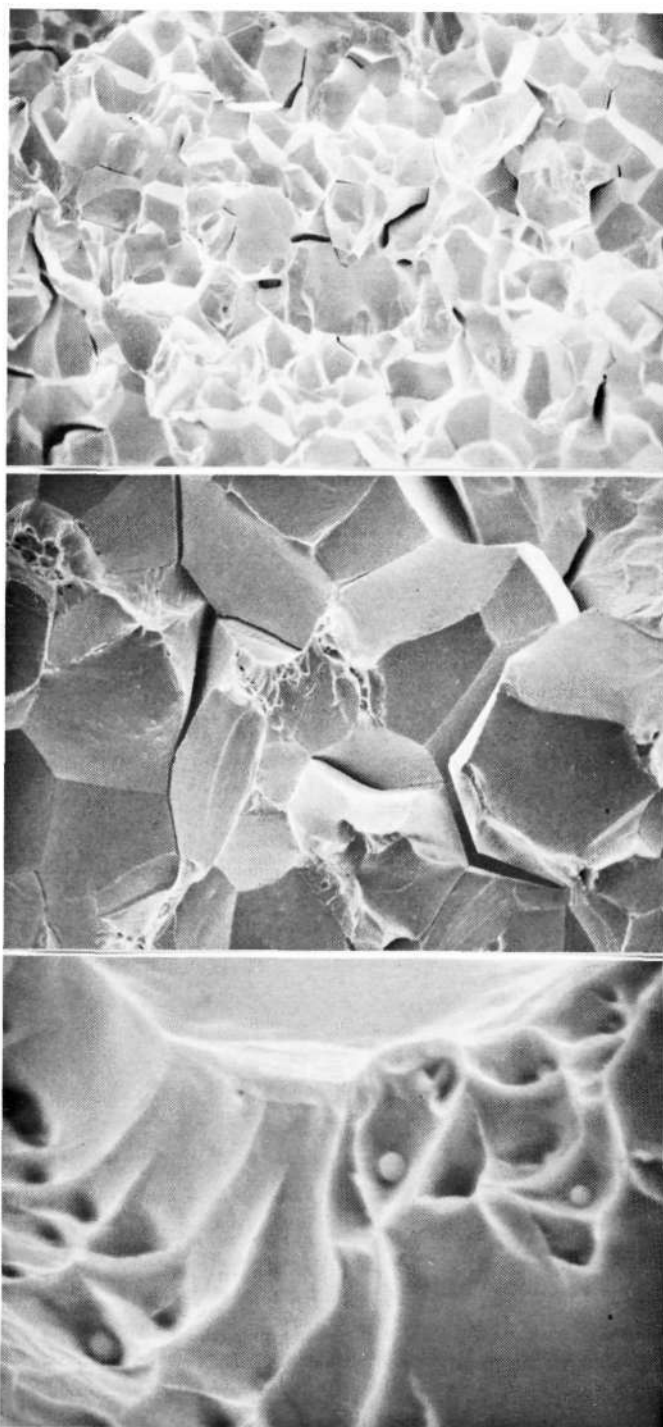
FIGURE 33. Transmission Electron Micrograph of GTA Weld Specimen 10.

Reproduced from
best available copy.



Aged 7500 Hours - 1038°C (1900°F)

FIGURE 34. As-Aged Microstructure of T-111 Tube Specimen 11.



160X

500X

5000X

Aged 7500 Hours - 1038°C (1900°F)

FIGURE 35. Scanning Electron Micrographs of Fracture Surface of T-111 Tube Specimen 11 ; Fractured at -196°C (-320°F).

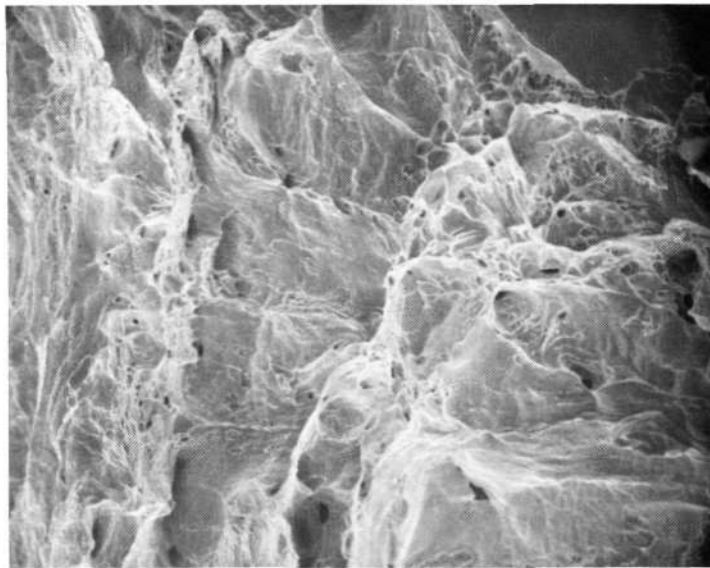
dimpled rupture. Precipitates were invariably associated with the dimpled regions. Micrographs of the Auger tested specimen, Figure 36, show a completely different picture. The fracture displays very high ductility, indicating failure occurred largely due to transgranular shear. The reason for this difference was not immediately obvious but three possible explanations were possible based on the slightly different pre-evaluation histories:

1. Bend fractures were performed at $-196^{\circ}\text{C}(-320^{\circ}\text{F})$ while Auger fractures were accomplished at $-150^{\circ}\text{C}(-238^{\circ}\text{F})$.
2. Bend-fracture specimens were full-section tube wall pieces (Figure 3) while the Auger specimens were surface ground prior to testing (Figure 4b). This suggested the possibility surface contamination was playing an important role.
3. The Auger specimens were annealed 1 hour at $982^{\circ}\text{C}(1800^{\circ}\text{F})$ after machining, to eliminate possible effects of the machining operation.

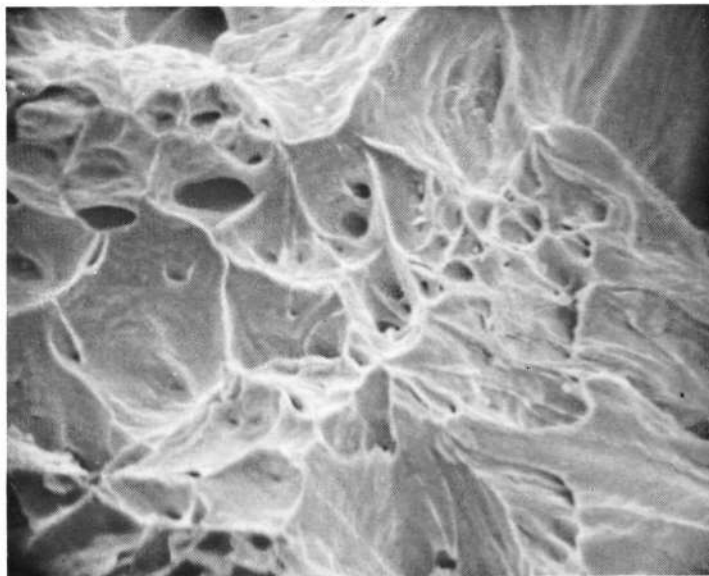
By preparing a series of full section tube wall specimens (Figure 4c) and testing in a controlled set of conditions we were able to establish the third possibility as responsible for the behavior observed. Hence, a specimen was prepared for Auger analysis without the use of a post-machine anneal. Following Auger analysis the fracture surface was examined by SEM, Figure 37. The fracture was 80-90% intergranular, in agreement with the specimen bend-fractured at $-196^{\circ}\text{C}(-320^{\circ}\text{F})$, Figure 35.

These results imply the notch-machining operation has a tremendous influence on the fracture behavior of this material. There have been other similar observations of the critical nature of the pre-test specimen preparation procedure and while the exact mechanism is not known the possibility of a hydrogen-like embrittlement effect is indicated.

Figure 38 is a transmission electron micrograph of a region near the fracture of the bend-fractured specimen. The structure shown is fairly typical of this material. Dislocation segments display a tendency to lie along preferred directions. Dipoles and some evidence of cross-slip can be seen.



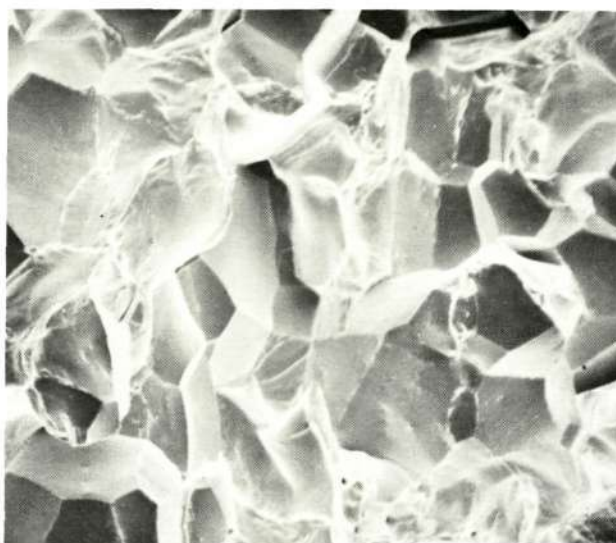
500X



2000X

Aged 7500 Hours-1038°C (1900°F)

FIGURE 36. Scanning Electron Micrographs of Fracture Surface of T-111 Tube Specimen 11 ; Fractured in Auger Apparatus at -150°C (-238°F). Annealed 1 Hour- 982°C (1800°F) Prior to Testing.



400X



400X

Aged 7500 Hours-1038°C (1900°F)

FIGURE 37. Scanning Electron Micrographs of Fracture Surface of T-111 Tube Specimen 11 ; Fractured in Auger Apparatus at -150°C (-238°F). Not Annealed Prior to Testing.



72-0027

0.2 μm

89,200X

Aged 7500 Hours-1038°C (1900°F)

FIGURE 38. Transmission Electron Micrograph of T-111 Tube Specimen 11.

Results of the Auger analysis of specimen 11 are presented in Table 4. Only the results of the re-test are provided since the failure to achieve intergranular separation the first time renders that data meaningless. The only significant segregation which could be detected at the grain boundaries was due to hafnium and possibly silicon. The high energy silicon peak almost exactly coincides with a strong hafnium peak, making accurate determination of trace amounts of silicon extremely difficult since only the rather weak silicon peak at 91 ev can be used. This was not a problem in specimens 3 or 10 (Table 3) since the silicon concentration was considerably greater.

Specimen 12. This specimen was removed from a segment of a loop which had been exposed to 1227°C (2240°F) for 10,000 hours. The microstructure of the as-exposed tubing is shown in Figure 39. Comparison to Figure 34 reveals a tremendous difference in the "cleanliness" of the two materials. The microstructure of specimen 12 is typical of "normal" T-111 -i.e T-111 which has not been exposed to compromising environments.

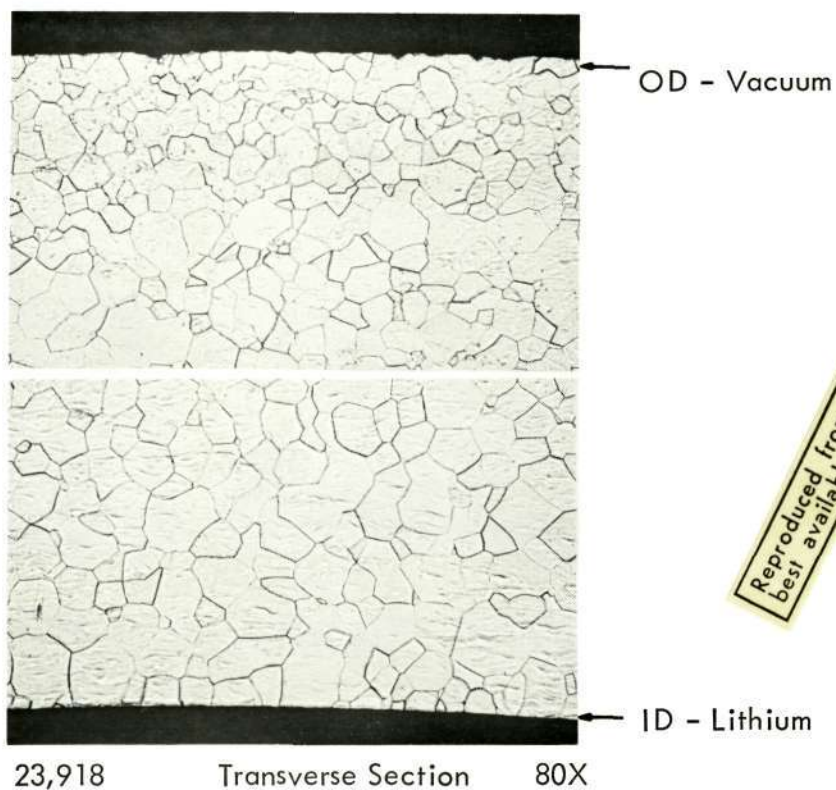
Scanning micrographs of the specimen bend-fractured at -196°C (-320°F) are presented in Figure 40. Fracture has occurred by a mixed mode, with regions of intergranular, cleavage and ductile rupture all present. As we found for specimen 11, the initial Auger specimen, which had been annealed 1 hour at 982°C (1800°F) prior to testing, failed by transgranular shear at very high ductility, Figure 41. Although not as dramatically different as for specimen 11, again a change in behavior was indicated.

Using the same procedure as for specimen 11, a series of full section tube wall specimens were prepared and tested. The second Auger-tested specimen, not given a pre-test anneal at 982°C (1800°F), displayed a fracture somewhat between that of the bend-fractured specimen and the previous Auger specimen, Figure 42. This implies that, although the pre-test anneal has some influence on the behavior, it is not nearly as profound as for specimen 11. Hence, it appears that:

Table 4. Results of Auger Analyses on T-111 Tubing Specimens

Specimen	Condition	Concentrations (a/o) (a)								
		Ta	Hf	W	C	O	N	F	K	Si
11	As-Fractured	70	6	5	6	11	1.5	0.2	0	0.6
12	As-Fractured	80	1	7	4	8	0	0.2	0	0

(a) Accuracy of concentrations $\pm 20\%$ of recorded values.



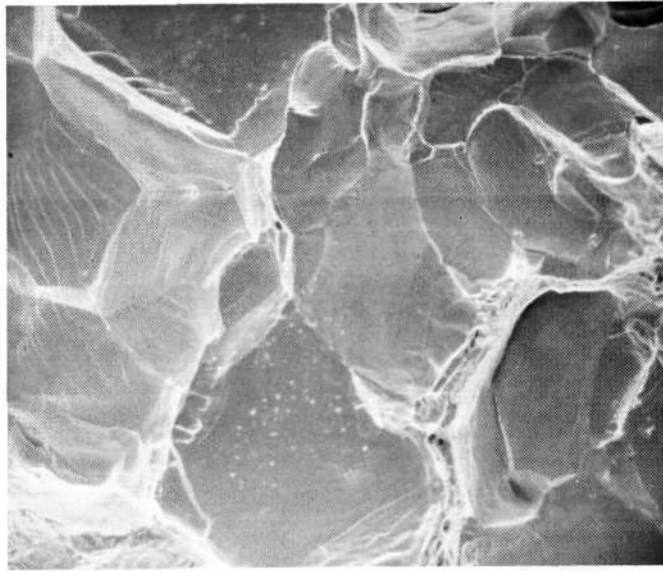
Reproduced from
best available copy.



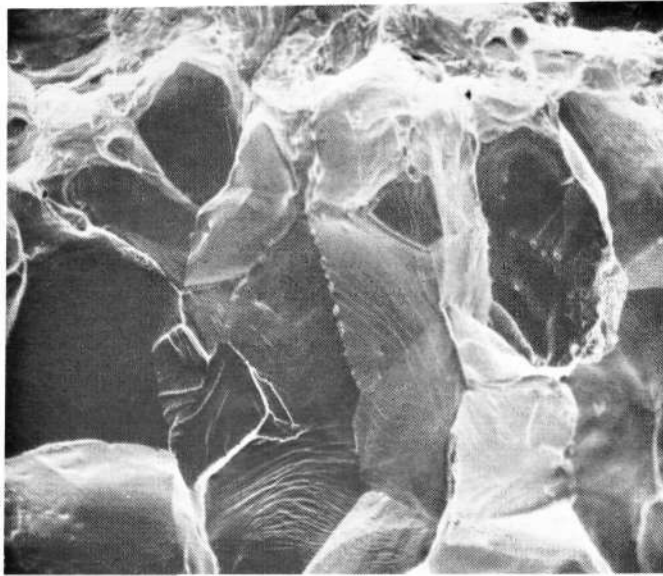
23,912 Transverse Section 750X

Aged 10,000 Hours - 1227°C (2240°F)

FIGURE 39. As-Aged Microstructure of T-111 Tube Specimen 12.



450X



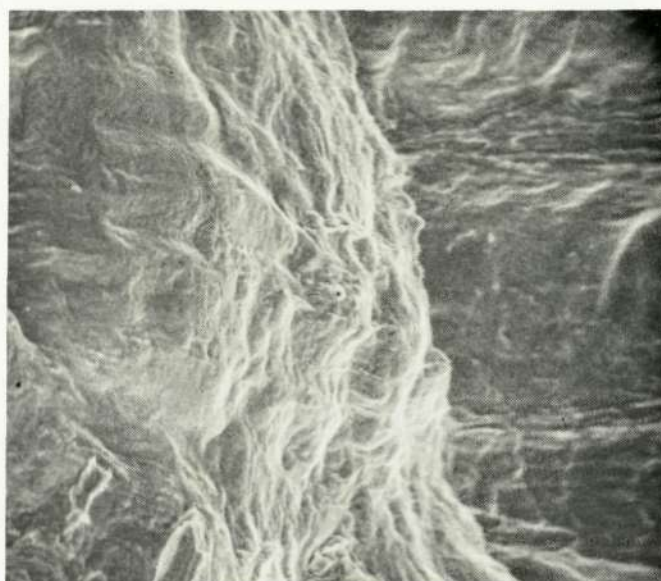
450X

Aged 10,000 Hours-1227°C (2240°F)

FIGURE 40. Scanning Electron Micrographs of Fracture Surface of T-111 Tube Specimen 12 ; Fractured at -196°C (-320°F).



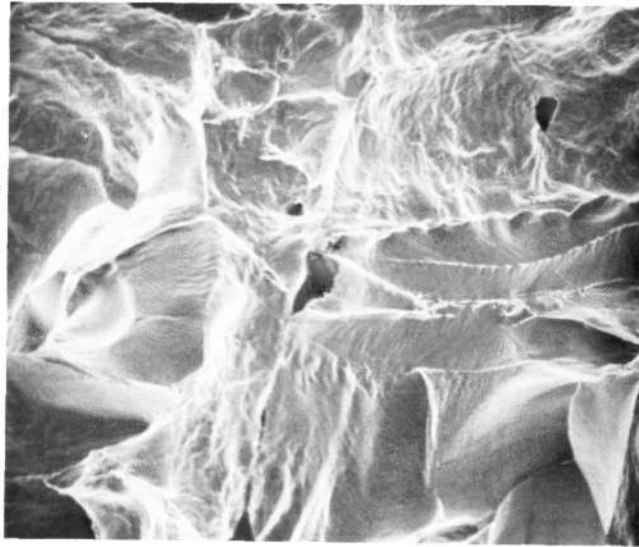
550X



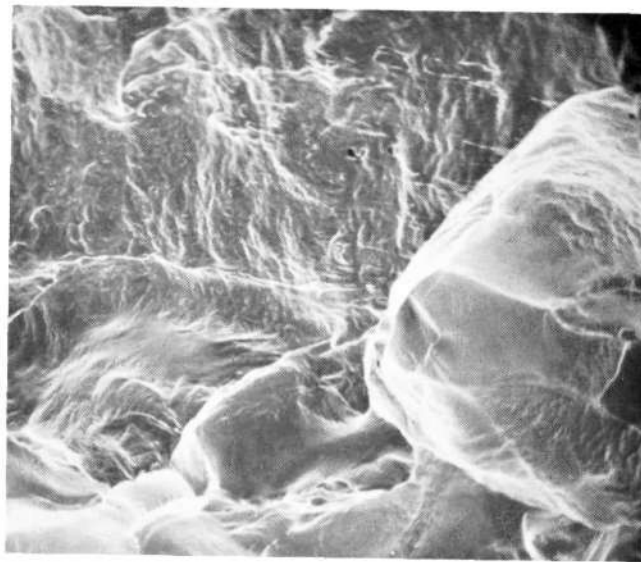
1100X

Aged 10,000 Hours-1227°C (2240°F)

FIGURE 41. Scanning Electron Micrographs of Fracture Surface of T-111
Tube Specimen 12 ; Fractured in Auger Apparatus at -150°C
(-238°F). Annealed 1 Hour-982°C (1800°F) Prior to Testing.



450X



450X

Aged 10,000 Hours - 1227°C (2240°F)

FIGURE 42. Scanning Electron Micrographs of Fracture Surface of T-111 Tube Specimen 12; Fractured in Auger Apparatus at -150°C (-238°F). Not Annealed Prior to Testing.

- (i) specimen 12 is less prone (than specimen 11) to the "hydrogen embrittlement effect" induced by the machining and cutting operations, and
- (ii) specimen 12 is approaching a true ductile-brittle transition in going to -196°C (-320°F) from -150°C (-238°F).

Examination of this specimen by TEM was limited by the fact only one good foil was obtained. This foil was prepared from a region right at the fracture and revealed a very high dislocation density. Only 1 or 2 very small, isolated grain boundary precipitates were observed.

The results of Auger analysis of specimen 12 are presented in Table 4. The low hafnium value and higher tungsten content than was found for the other Auger specimens is in agreement with the SEM observations of non-intergranular fracture. This specimen had the lowest concentration of impurities of all the T-111 specimens analyzed by Auger electron spectroscopy on this program.

5.0 DISCUSSION

5.1 Aged GTA Sheet Welds

A summary of the fracture behavior of the aged GTA sheet weld specimens is presented in Table 5. Percentages of the various fracture modes were estimated from the SEM studies of the fracture surfaces. In interpreting the data of Table 5 an extremely important point to keep in mind is that specimens were force-fractured. For several this required repeated reverse bending at -196°C (-320°F). Hence, the fact that cleavage was observed on the fracture surfaces does not necessarily imply truly brittle behavior. In many cases, the choice between cleavage and a more ductile failure mode appeared the result of local orientation.

The effect of the 1 hour- 1982°C (3600°F) post-age anneals has been largely to "normalize" the fracture behavior. That is, specimens 2,5,7 and 9 display very similar fracture characteristics despite the fact their companion specimens, not post-age annealed, exhibited fractures ranging from >95% intergranular to 100% shear.

Contrary to general expectations, the presence of large, discrete HfO_2 precipitates at the grain boundaries seems to promote localized ductile rupture. Evidence of this was noted even on fracture surfaces predominantly intergranular, Figure 13. The mechanism by which this occurs is well established^(11,12). During the plastic deformation of materials containing inclusions and incoherent precipitates, microvoids or free surfaces form at the second phase-matrix interface due to differences in the elastic and plastic properties. As deformation proceeds the cavities are enlarged until the remaining matrix becomes constricted in the inter-cavity regions. Rupture ultimately occurs when the remaining matrix regions can no longer support the applied stress.

From the TEM studies we are able to conclude that, with the exception of possible coarsening of the grain boundary oxide precipitates, no general aging reaction is occurring. The low dislocation density observed in most specimens may not be of particular significance

Table 5. Summary of GTA Weld Specimen Fracture Behavior.

Specimen	Fracture Temp. °C(°F)	Fracture Mode (a)			Major Auger Results ^(b)
		IG	CI	Duct.	
1	-196(-320)	>95		<5	3 F ; up to 6.5 K
1 Auger	-150(-238)	>90	5	<5	
2	-196(-320)		70	30	
3	-196(-320)	>95		<5	6 Si ; Trace F , K
3 Auger	-150(-238)	>90	5	<5	
4	-196(-320)			100	
5	-196(-320)		60	40	
6	-196(-320)		70	30	
7	-196(-320)		60	40	
8	-196(-320)		50	50	
9	-196(-320)		35	65	1.5 Si ; Trace F , K
10	-196(-320)	>95		<5	
10 Auger	-150(-238)	>90	5	<5	

(a) IG = intergranular

CI = cleavage

Duct. = ductile

Values are approximate %'s based on SEM results.

(b) For details see Table 3, page 23.

See Table 1, page 9 , for thermal histories of specimens.

since this will be at least partially dependent on the distance from the fracture to the region from which foils were prepared. However, the lack of matrix precipitation and the absence of dislocation-grain boundary precipitate interactions are significant.

To lend perspective to the data of Table 5 recall that specimen 6 showed no indication of a ductility limitation to temperatures as low as -196°C (-320°F), Table 1. This suggests that in "normal" 1t bend testing (i.e. no repeated reversal of bending or force fracturing) no loss of ductility would be observed for specimens 2, 4-9. Only specimens 1,3 and 10 display what appears to be true ductility impairment. These specimens do not represent unique conditions of thermal exposure. Hence, it is doubtful that thermal response of the microstructure is responsible for the effects observed.

The results of Auger analysis of the fracture surfaces which were presented in Table 3, and the highlights of which are included in Table 5, suggest segregation of contaminants as a possible explanation for the behavior of specimens 1, 3 and 10. No experience exists with regard to the effect of fluorine, potassium or silicon in tantalum-base alloys. Nevertheless, lacking evidence to the contrary, the presence of these "foreign" elements appears to be adversely affecting the cohesive properties of the grain boundaries sufficiently to favor the observed intergranular fracture mode.

Fluorine almost certainly is present from the pickling and cleaning operations which employ hydrofluoric acid. It is much more difficult to explain the presence of potassium and silicon. Since some specimens from the same heats of T-111 as those exhibiting intergranular fracture were not prone to that problem we can conclude that contamination, at whatever stage of the alloy's history it was introduced, is a localized condition. In this respect the aging treatments may be serving a secondary role in that segregation of these impurities to the fusion zone grain boundaries could conceivably be enhanced by prolonged elevated temperature exposures.

In summary, no evidence of a "classical" aging reaction occurring in the welds due to long-time thermal exposures was obtained. Rather, it appears that random intergranular fracture behavior is related to the presence of potassium, silicon and fluorine at the fusion zone grain boundaries of the specimens affected. The more sophisticated analytical procedures used in the present program have provided information which largely discredits the earlier interpretation of aging in T-111 GTA welds (Contract NAS 3-2540⁽¹⁾) which was based on an extensive fusion zone precipitation reaction.

5.2 Aged T-111 Tubing

The fracture behavior of the aged tube specimens 11 and 12 is summarized in Table 6. The difference in behavior of the two Auger specimens appears to be solely the result of a one hour-982°C (1800°F) post-machine annealing treatment. A complete reversal in behavior is indicated, implying that something is occurring during the machining process which is causing a marked shift to intergranular fracture. This effect has been noted previously whereby T-111, particularly after long-time aging at temperatures near 1038°C (1900°F), is prone to a hydrogen-like embrittlement effect of cut, polished, or metallographically prepared in the presence of aqueous solutions and subsequently stressed⁽³⁾. More recently in tests conducted at NASA Lewis⁽¹⁾, the NASA investigators also have shown that, even if strictly dry pre-test conditions are observed, the presence of small amounts of moisture in the test atmosphere is sufficient to cause erratic bend behavior in T-111 aged at 1038°C (1900°F).

An important aspect of the results of evaluations on specimen 11 was the observation that, despite apparently high oxide precipitate density at the grain boundaries, proper pre-test handling and testing procedures permit ductile behavior of this material to temperatures at least as low as -150°C (-238°F).

Table 6. Summary of T-111 Tube Specimen Fracture Behavior.

Specimen	Fracture Temp. °C (°F)	Fracture Mode (b)			Major Auger Results ^(c)
		IG	CI	Duct.	
11	-196(-320)	>90		<10	Only matrix & interstitials Trace F, Si
11 Auger ^(a)	-150(-238)		10	90	
11 Auger	-150(-238)	80	10	10	
12	-196(-320)	40	40	20	Very weak F , K Very weak F
12 Auger ^(a)	-150(-238)			100	
12 Auger	-150(-238)	10	20	70	

(a) These specimens were post-machine annealed 1 hour-982°C(1800°F) prior to testing.

(b) IG = intergranular

CI = cleavage

Duct. = ductile

Values are approximate %'s based on SEM results.

(c) For details see Table 4, page 62.

See Table 1, page 9 , for thermal histories of specimens.

Although a similar sensitivity to pre-test handling was noted for specimen 12, the effect is less dramatic than for specimen 11. Although chemical analyses was not available for these specimens, chemical analysis of materials close to these in the test loops showed specimen 11 to be higher in interstitials than specimen 12⁽¹⁴⁾. The fact that considerable ductility was observed at -150°C (-238°F) even in material not post-machine annealed coupled with the observation of about 40% intergranular fracture at -196°C (-320°F) for the same material suggests the following:

- (i) specimen 12 is less prone to the embrittling effect induced by improper pre-test handling than is specimen 11, and
- (ii) we appear to be approaching a true ductile-brittle transition in this material as we approach -196°C (-320°F).

Based on microstructural observations, there does not appear to be anything unique about the 1038°C (1900°F) aging temperature which by itself renders T-111 aged at that temperature more susceptible to intergranular failure than material aged at any other temperature. Comparison of the microstructure of specimen 11 (aged at 1038°C) with that of specimen 12 (aged at 1227°C) does reveal a significant difference in quantity of HfO_2 precipitate which could be due to poorer quality starting material, operation in an inadequate vacuum, or characteristic of the mass transfer kinetics at those particular sections of the loop.

Specimen 11 has undergone apparent oxygen contamination during operation. Oxygen has been shown to degrade the low temperature ductility of T-111 when introduced into the T-111 matrix during low temperature ($< 1100^{\circ}\text{C}$) low oxygen partial pressure oxidation^(15, 16, 17).

The loss in low temperature ductility results from the potent strengthening of the matrix by the coherent hafnium oxide precipitate which causes an increase in the DBTT. However, the recovery of low temperature ductility in specimen 11 after a subsequent one hour anneal

at the operating temperature of 1038°C (1900°F) most likely precludes this as the responsible cause.

Although no direct metallographic evidence was observed, the sensitivity of T-111 aged at 1038°C (1900°F) to post-age handling in moist environments does suggest a discontinuous phenomena such as an allotropic transformation. Hafnium is completely soluble in tantalum at 1800°C and above, but the Ta-Hf phase diagram does show a miscibility gap with a monotectoid decomposition reported to occur at 1050°C (1922°F) where $\beta\text{Ta} + \beta\text{Hf} \rightarrow \beta\text{Ta} + \alpha\text{Hf}$ ⁽¹⁸⁾. (At the monotectoid temperature of 1050°C, the solubility of hafnium in tantalum is approximately 12 atom percent.) This monotectoid decomposition reaction may explain why T-111 is apparently more sensitized to hydrogen embrittlement after aging at 1038°C (1900°F) than at any higher temperature. However, results of this program do show that proper handling before and during post-age testing of T-111 can result in quite ductile behavior.

6.0 CONCLUSIONS

The results of this investigation allow the following conclusions:

Aged GTA Sheet Welds

1. No classic aging temperature range exists from 982°C (1800°F) through 1316°C (2400°F) which results in a propensity for intergranular failure at low temperature.
2. No evidence was obtained to support the possibility of an aging reaction occurring in weld specimens exposed for long times in the temperature range 982°C (1800°F) through 1316°C (2400°F).
3. Precipitation was largely confined to the presence of coarse HfO_2 precipitates at the grain boundaries. Very little intragranular precipitation was observed.
4. Dislocation densities were quite low after bend testing at -196°C (-320°F) with very little evidence of dislocation-precipitate or dislocation-grain boundary interactions.
5. Auger electron emission spectroscopy, performed on freshly fractured surfaces, revealed significant concentrations of silicon, potassium and fluorine at the grain boundaries of specimens displaying a tendency toward low temperature intergranular fracture.

Aged T-111 Tube Specimens

6. The results of this program indicate thermal exposure at 1038°C (1900°F) causes a greater sensitivity to subsequent "hydrogen embrittlement effects" induced by machining or cutting operations than exposure for long times at 1227°C (2240°F). With proper handling, material aged at both of these conditions displayed ductile behavior to temperatures at least as low as -150°C (-238°F).
7. Despite HfO_2 precipitates at grain boundaries, specimen 11, exposed to lithium for 7500 hours at 1038°C (1900°F), behaved in a ductile manner at -150°C (-238°F) when normal precautions were taken in pre-test handling procedures.

8. Except for the possibly high oxygen level in specimen 11, Auger electron emission spectroscopy revealed no significant contamination had resulted from the long-time exposures to lithium in the temperature range 1038°C (1900°F) to 1227°C (2240°F).
9. The presence of HfO_2 precipitation along grain boundaries, does not necessarily imply premature intergranular fracture at low temperatures.
10. Results of this study concur with those conducted at NASA Lewis with regard to sensitivity of aged T-111 to testing (and pre-test handling) environment.

7.0 RECOMMENDATIONS

The conclusions indicate that the low temperature ductility of T-111 base metal and weld metal is not adversely affected after long time thermal exposure in the temperature range of 982°C (1800°F) through 1316°C (2400°F). However, it was indicated that T-111 aged at 1038°C (1900°F) is sensitive to post-age handling procedures which give rise to a hydrogen embrittlement effect. To more precisely define the mechanism(s) by which this apparent discontinuous phenomenon occurs, the following additional investigative work is recommended:

- determine the kinetics and precise temperature or temperature range at which T-111 becomes sensitized to post-age handling.
- investigate the effects of other interstitial additions such as nitrogen, oxygen, and carbon on the "sensitization" reaction.
- investigate the fracture mode and determine the temperature dependence of fracture for "sensitized T-111 under controlled environmental test conditions.

8.0 REFERENCES

1. Lessmann, G.G. and Gold, R.E. , "Long-Time Elevated Temperature Stability of Refractory Metal Alloys", Part II of "Determination of Weldability and Elevated Temperature Stability of Refractory Metal Alloys", NASA CR-1608, September, 1970.
2. Gold, R.E. and Lessmann, G.G., "Influence of Restraint and Thermal Exposure on Welds in T-111 and ASTAR-811C", NASA CR-72858, January, 1971.
3. Quarterly Progress Reports on Contract NAS 3-6474, "Advanced Refractory Alloy Corrosion Loop Program", Work conducted by General Electric, Nuclear Systems Programs, Cincinnati, Ohio. Report numbers
 GESp-562, NASA CR-72818, November 1970
 GESp-606, NASA CR-72853, February 1971
 GESp-652, NASA CR-72985, May 1971
4. Burhop, E.H.S., The Auger Effect and Other Radiationless Transitions, University Press, England.
5. Listengarten, M.A., Bulletin Acad. Sci. USSR, Physical Series, 24 , p. 1050 (1960).
6. Stein, D.F., Joshi, A. and LaForce, R.P., "Studies Utilizing Auger Electron Emission Spectroscopy on Temper Embrittlement in Low Alloy Steels, Trans. ASM, 62, pp. 776-783 (1969).
7. Marcus, H.L. and Palmberg, P.W., "Auger Fracture Surface Analysis of a Temper Embrittled 3340 Steel," Trans AIME, 245 , pp.1664-1666 (1969).
8. Joshi, A. and Stein, D.F., "Intergranular Brittleness Studies in Tungsten Using Auger Spectroscopy," Metall. Transactions, 1 , pp. 2543-2546 (1970).
9. Viswanathan, R., "Temper Embrittlement in a Ni-Cr Steel Containing Phosphorus as Impurity", Metall. Transactions, 2 , pp. 809-815 (1971).
10. Stein, D.F. Weber, R.E. and Palmberg, P.W., "Auger Electron Spectroscopy of Metal Surfaces," Journal of Metals, February 1971 .
11. Beachem, C.D. and Pelloux, R.M.N. , "Electron Fractography - A Tool for the Study of Micromechanisms of Fracturing Processes," ASTM Special Technical Publication No. 381, pp. 210-245 (1965).

12. Schmitt-Thomas, K., Klingele, H. and Woitscheck, A. , "The Micromorphology of Metallic Fractures," Practical Metallography, Special Issue 2 on Applied Electron Metallography, pp. 102-124 (1970).
13. Watson, G. K. , and Stephens, J. R. , "Effect of Aging at 1040°C (1900°F) on the Ductility and Structure of a Tantalum Alloy, T-111", NASA TN-D-6988, October 1972.
14. Final report on Contract NAS 3-6474, "T-111 Rankine System Corrosion Loop".
15. Fuels and Materials Development Program Quarterly Progress Report for Period Ending December 31, 1971. ORNL-TM-3703.
16. Stoner, D. R. , "Determination of Weldability and Elevated Temperature Stability of Refractory Metal Alloys - Part III Effect of Contamination Level on Weldability of Refractory Metal Alloys", NASA CR-1609.
17. Buckman, R. W. Jr. , Unpublished research on status of internally oxidized T-111 alloy, Westinghouse Astronuclear Laboratory.
18. Anon: "Binary and Ternary Phase Diagram of Columbium, Molybdenum, Tantalum, and Tungsten", DMIC Report No. 152, April 28, 1961.

DISTRIBUTION LIST

DO NOT PAINT

NASA Lewis Research Center
21000 Brookpark Road
Cleveland, Ohio 44135

Attn: P. E. Moorhead, MS 106-1 (3)
R. L. Davies, MS 106-1
N. T. Saunders, MS 105-1
S. S. Manson, MS 49-1
R. E. Gluyas, MS 105-1
R. W. Hall, MS 105-1
W. D. Klopp, MS 105-1
C. M. Scheuermann, MS 106-1
R. E. English, MS 500-201
R. Brietweiser, MS 302-1
S. Kaufman, MS 49-2
M. Krasner, MS 49-2
A. Lietzke, MS 49-2
P. Donoughe, MS 49-2
F. Rom, MS 106-1
Tech. Util. Ofc., MS 3-19
G. M. Ault, MS 3-13
E. Kolman, MS 500-313
Report Control, MS 5-5
Patent Counsel, MS 500-311
Library, MS 60-3
G. K. Watson, MS 105-1
J. R. Stephans, MS 105-1
L. Rosenblum, MS 302-1

NASA Headquarters
Washington, D. C. 20546

Attn: Librarian
NS-1/C. Johnson
RW/G. Deutsch
RWM/J. Gangler
NS-1/R. Anderson
NS-1/R. Miller

NASA Lewis Research Center
Plum Brook Station
Taylor and Columbus Rds.
Sandusky, Ohio 44870

Attn: Librarian
H. B. Barkley
D. Reilly

NASA Ames Research Center
Moffett Field, Calif. 94055
Attn: Librarian

NASA Jet Propulsion Laboratory
4800 Oak Grove Drive
Pasadena, Calif. 91103
Attn: Librarian
J. Mondt, 122-123
W. Phillips

NASA Langley Research Center
Hampton, Virginia 23365
Attn: Librarian
W. Brooks
B. Stein

NASA Manned Spacecraft Center
Houston, Texas 77058
Attn: Librarian
R. Johnson

NASA George C. Marshall
Space Flight Center
Marshall Space Flight Center, Ala. 35812
Attn: Librarian
G. Riehl
G. McKannon
G. Cataldo

NASA Scientific and Technical
Information Facility
P. O. Box 5700
Bethesda, Maryland
Attn: NASA Representative

AiResearch Mfg. Co.
Sky Harbor Airport
402 South 36th St.
Phoenix, Arizona 85041
Attn: Librarian

AiResearch Mfg. Co.
9851-9951 Sepulveda Blvd.
Los Angeles, Calif. 90045
Attn: Librarian

Argonne National Laboratory
9700 South Cass Ave.
Argonne, Ill. 60439
Attn: Librarian

Amy Ordnance Frankford Arsenal
Bridesburg Station
Philadelphia, Pa. 19137
Attn: Librarian

Atomics International
8900 DeSoto Ave.
Canoga Park, Calif.
Attn: Librarian
T. Moss
W. Botts
H. Pearlman

Bureau of Ships
Dept. of the Navy
Washington, D. C. 20390
Attn: Librarian

Battelle Memorial Institute
Columbus Laboratories
Columbus, Ohio 43201
Attn: Librarian
D. L. Keller
P. Gripshover
B. Wilcox

Battelle Memorial Institute
Pacific Northwest Laboratories
Richland, Washington
Attn: Librarian

Boeing Aircraft Corp.
Seattle, Washington 98124
Attn: Librarian

Bureau of Weapons
Research and Engineering
Material Division
Washington, D. C. 20390
Attn: Librarian

Brookhaven National Laboratory
Upton, Long Island, N. Y. 11973
Attn: Librarian

Chance Vought Aircraft, Inc.
P. O. Box 4907
Dallas, Texas 75222
Attn: Librarian

Clevite Corp.
Mechanical Research Div.
540 East 105th St.
Cleveland, Ohio 44108
Attn: Librarian

Convair Astronautics
5001 Kerny Villa Rd.
San Diego, Calif. 92111
Attn: Librarian

Electro-Optical Systems, Inc.
Advanced Power Systems Div.
Pasadena, Calif. 91105
Attn: Librarian

Fansteel Metallurgical Corp.
North Chicago, Ill. 60064
Attn: Librarian
A. Dana

Ford Motor Co.
Aeronutronics
Newport Beach, Calif. 92660
Attn: Librarian

General Electric Co.
Vallecitos Atomic Laboratory
Pleasanton, Calif. 94566
Attn: Librarian

University of Michigan
Dept. of Chemical & Metallurgical Engrg.
Ann Arbor, Mich. 48105
Attn: Librarian

U. S. Atomic Energy Commission
Washington, D. C. 20525
Attn: Tech. Reports Librarian
J. Simmons
C. Tarr
N. Goldenberg
A. Littman
E. Hoffman

U. S. Atomic Energy Commission
Technical Information Service Ext.
P. O. Box 62
Oak Ridge, Tenn. 37831 (3)

U. S. Naval Research Laboratory
Washington, D. C. 20390
Attn: Librarian

Vought Astronautics
P. O. Box 5907
Dallas, Texas 75222
Attn: Librarian

Wah Chang Corp.
Albany, Oregon 97321
Attn: Librarian
S. Worcester

Westinghouse Electric Corp.
Aerospace Electric Division
P. O. Box 989
Lima, Ohio 45802

Westinghouse Electric Corp.
Research Laboratories
Churchill Boro
Pittsburgh, Pa. 15235
Attn: Librarian
R. T. Begley

Wolverine Tube Division
Calumet and Hecla, Inc.
17200 Southfield Rd.
Allen Park, Mich. 48101
Attn: E. F. Hill

Wright Patterson Air Force Base
Air Force Materials Laboratory
Dayton, Ohio 45433
Attn: N. Geyer
T. Cooper
Librarian
J. L. Morris
H. J. Middendorp, ASNRC 33143
C. L. Hamsworth

Wyman-Gordon Co.
North Grafton, Mass. 01536
Attn: Librarian